TRANSIENT ABSORPTION SPECTROSCOPY

USING

TUNABLE DIODE LASERS

TRANSIENT ABSORPTION SPECTROSCOPY USING TUNABLE DIODE LASERS

by

JOSEPH EDWARD HAYWARD, B. Eng.

A Thesis

Submitted to the School of Graduate Studies

in Partial Fulfilment of the Requirements

for the Degree

Master of Engineering

McMaster University

September 1988

MASTER OF ENGINEERING McMASTER UNIVERSITY

(Engineering Physics) Hamilton,Ontario

TITLE: Transient absorption spectroscopy using tunable diode lasers.

AUTHOR: JOSEPH EDWARD HAYWARD, B. Eng. (McMaster University)

SUPERVISORS: Professor J. Reid and Professor D.T. Cassidy

NUMBER OF PAGES: xv, 71

ABSTRACT

This thesis describes experimental techniques which have been developed to monitor transient infrared absorptions using lead–salt tunable diode lasers. The techniques are easily implemented, yield sensitivities which are limited by detector noise at 10^{-5} level of absorbance, and have a response time on the order of one microsecond. The transient absorption detection techniques are essentially high frequency versions of the sweep integration technique. TDL modulation rates of 100 kHz and 500 kHz allow for absorption sampling rates of 200 kHz and 500 kHz respectively. In order to reproducibly achieve near–detector–noise–limited sensitivities for 100 kHz TDL modulation rates, an automated analog subtraction circuit has been developed which removes the effects of minor TDL power variations. At the 500 kHz modulation rate digital filtering techniques are used to remove the effects of this power variation.

The transient absorption detection technique could become an important tool for the detection of unstable species such as free radicals or molecular ions. The spectroscopy of these transient species could reveal new insights in important research areas such as atmospheric and interstellar chemistry, biology and semiconductor materials processing.

In addition, the theoretical aspects of noise reduction techniques commonly used in the area of laser spectroscopy are examined in this thesis. Using a Gaussian statistical analysis, the theoretical relationships for both bandwidth limiting and digital averaging noise reduction methods are experimentally confirmed.

ACKNOWLEDGEMENTS

I would like to express my gratitude to my supervisors, Dr. John Reid and Dr. Dan Cassidy for their guidance and patience throughout the course of this work.

I would also like to thank my family and friends for their continued support of all of my endeavours. A special thanks to my wife Isabel, who has kept me sane ever since I started at McMaster.

This thesis is dedicated to the memory of those who, in one way or another, have touched me in special ways: Edward Jesse Cowell, Joseph Henry Hayward, Florence Harriet Hayward, Francis Bromfield, Delores Runnalls and Jean McCreary.

This work was supported, in part, by the Natural Sciences and Engineering Research Council of Canada.

TABLE OF CONTENTS

		PAGE
LIST OF FIGURES		vii
CHAPTER 1	INTRODUCTION	1
CHAPTER 2	GENERAL CHARACTERISTICS OF LEAD–SALT TUNABLE DIODE LASERS	5
2.1	Introduction	5
2.2	Material Considerations, Structure and Lasing Properties of TDL's	5
2.3	Wavelength Tuning of TDL's	11
2.4	Effect of TDL Modulation in the Vicinity of an Absorption Line	13
2.5	Summary	15
CHAPTER 3	HIGH SENSITIVITY DETECTION OF TRANSIENT INFRARED ABSORPTIONS	16
3.1	Introduction	16
3.2	Experimental Apparatus	17
3.3	Transient Absorption Results for 100 kHz TDL Modulation Rates	27
3.4	Transient Absorption Results for 500 kHz TDL Modulation Rates	31
3.5	Sensitivity of the Transient Absorption Detection Technique	36

3.6 Summary 38

CHAPTER 4 NOISE REDUCTION TECHNIQUES FOR SPECTROSCOPY 41

4.1 Introduction 41

4.2 The Nature of White Noise 42

4.3 Noise Reduction by Bandwidth Limiting 48

4.4 Noise Reduction by Digital Averaging 56

4.5 Bandwidth Reduction versus Digital Averaging 62

4.6 Summary 65

CHAPTER 5 CONCLUSION 66

REFERENCES 68

LIST OF FIGURES

		Page
Figure 2–1:	Variation of energy gap (E_g), lattice constant (a) and refractive index (n) as a function of the lead–salt alloy composition at 77K. (Adapted from [13].)	7
Figure 2–2:	Resonance wavelengths of several important molecules which are often used in infrared spectroscopy. Also indicated are the wavelength regions which can be attained by compositional tuning of several lead–salt laser systems. (Adapted from [14].)	8
Figure 2–3:	Schematic diagram of a typical lead–salt diode laser. (Adapted from [14].)	10
Figure 2–4:	An idealised plot of the laser emission frequency as a function of current. Continuous optical tuning ranges are separated by discrete wavelength jumps known as "mode hops".	12
Figure 2–5:	Idealised plot of the detected optical power as the laser frequency tunes through a Doppler–broadened	14

absorption line. An applied current modulation to the TDL results in a detector signal which consists of both amplitude and optical frequency modulation effects. The resultant detector signal shows the absorption line superimposed upon the background AM component.

Figure 3–1: Schematic diagram of the apparatus used for the creation and monitoring of transient absorptions. The discharge tube contains a flowing mixture of N_2O in He at a total pressure of approximately 10 Torr. The discharge current is pulsed at a repetition frequency of 10 Hz. Each current pulse lasts for 200 μs and has a peak current of 250 mA. 18

Figure 3–2: Schematic diagram and frequency response of the bias–T insertion circuit. This circuit allows a DC bias current and an AC modulation signal to be combined and subsequently applied to the diode laser. The frequency response curve is measured at the output of the bias–T circuit across a simulated laser diode consisting of a 1 Ω resistor in series with a silicon diode. 20

Page

Figure 3–3: Conventional TDL scan of room temperature N_2O. The line marked "L" has a line–centre absorption of 1.6 %. Also shown in the inset is an energy level diagram of the N_2O molecule indicating the transitions relevant to the experiment. Line "L" is the R(35) line of the $(00^0 0 - 10^0 0)$ band of $^{14}N_2{}^{18}O$. The electric discharge places a transient population in level $02^0 1$, and this population creates a transient absorption on the P(8) transition of the $(02^0 1 - 12^0 1)$ band of $^{14}N_2{}^{16}O$ at 1273.527 cm^{-1}. 22

Figure 3–4: Idealised schematic which shows the technique of analog subtraction. The detector signal consisting of an absorption line superimposed upon an AM background component is combined with a sine wave at the inputs of a differential amplifier. Proper adjustment of the phase and amplitude of the sine wave from the phase–locked generator ideally results in an output signal which solely consists of the absorption signal. 24

Figure 3–5: Result of modulating the TDL at 100 kHz across line "L" of Fig. 3–3. Trace A is the output from 26

the HgCdTe detector. The N_2O absorption line is seen superimposed on the sinusoidal AM background signal and is displayed twice per modulation cycle. The lower trace shows the resultant signal after analog subtraction. The differential lineshape is the result of a high pass filter on the input of the video differential amplifier.

Figure 3–6: Demonstration of the high sensitivity transient detection technique for a 100 kHz TDL modulation rate. The TDL is tuned near the $(02^{0}1 - 12^{0}1)$ P(8) transition. Transient absorption is created on this transition by the discharge current pulse which starts at the time indicated by the dashed line. Each trace is the average of 1000 individual scans recorded by the digital oscilloscope. Trace A is recorded with the discharge firing and Trace B is recorded without exciting the discharge. Upon digital subtraction, the lower trace displays the weak absorption line increasing in strength as the current populates the $02^{0}1$ level. 28

Figure 3–7: Demonstration of the near detector–noise limited sensitivity of the transient absorption detection 30

technique for a 100 kHz TDL modulation rate. Trace A is reproduced from Fig. 3–6 and shows the detection of a transient infrared absorption. The first half of Trace B shows the limiting noise level inherent in the experiment whereas the second half of the trace shows the intrinsic detector noise for comparison purposes. If the lock–in amplifier is not used to track small TDL power variations, Trace C indicates that the noise after the analog and digital subtraction steps consists of an unwanted 100 kHz component. This "fundamental feedthrough" component has a magnitude equivalent to 8×10^{-3} % of the total TDL optical power.

Figure 3–8: Demonstration of the high sensitivity transient absorption detection technique for a 500 kHz TDL modulation rate. After digital subtraction of the records A and B, the resultant signal shown in Trace C reveals the transient absorption superimposed upon a 500 kHz component. This fundamental frequency component is caused by TDL power variations during the time it takes to capture the records which are to be digitally subtracted. 33

Page

Figure 3–9: Removal of the fundamental component using digital filtering techniques. Trace A is reproduced from Fig. 3–8 and shows the transient absorption line superimposed upon the unwanted 500 kHz component. Transforming to the frequency domain using standard FFT techniques produces the real and imaginary frequency component shown in Trace B. Retaining only those frequency components between the filter bars (800 kHz to 3 MHz) results in digital filtering of the original waveform. Returning to the time domain via an additional Fourier transform reveals the well–resolved transient absorption shown in Trace C. 34

Figure 3–10: Demonstration of the near detector–noise limited sensitivity of the transient absorption detection technique. Trace A is reproduced from Fig. 3–9 and shows the detection of a transient absorption at the 500 kHz TDL modulation rate. The first half of Trace B indicates the limiting noise level inherent in the experiment after analog subtraction, digital subtraction and digital filtering. The second half of 35

Trace B shows the intrinsic detector noise for comparison purposes.

Figure 4–1: Schematic diagram of a phase–sensitive detector. An input signal of frequency f_s is mixed with a reference signal of frequency f_o. The output of the phase–sensitive detector consists of the portion of the difference frequency which is within the bandwidth of the low–pass filter. 49

Figure 4–2: Schematic diagram of the experimental apparatus used to verify the theoretical noise reduction relationships. 51

Figure 4–3: Demonstration of the Gaussian voltage distribution of band–limited white noise. The voltage distribution of noise records subjected to filtering with a time constant of 3 msec is represented by the Gaussian distribution with the larger standard deviation (1.96 V). Subjecting the white noise to a filter with a larger time constant of 10 msec results in a decrease in the Gaussian standard deviation (1.25 V). The data points were obtained by generating a count versus voltage histogram for 53

10,000 noise voltage samples. The solid lines connecting the data points represent the best–fit Gaussian distributions which were calculated using a weighted least–squares algorithm. The inset of this figure shows 100 point portions of the 10,000 sample noise records used to generate the histogram values. (The data points and best–fit distributions have been normalized so that the areas under each Gaussian are identical.)

Figure 4–4: Demonstration of the relationship between the RMS noise voltage at the output of the lock–in amplifier and the time constant of the low–pass filter. Plotting the logarithm of the RMS noise voltage as a function of the logarithm of the time constant yields the data points indicated on the graph for both 6 dB and 12 dB/octave filter responses. The solid lines represent linear least–squares approximations to the respective data points. Calculated values of the slopes and intercepts of the best–fit lines are also indicated on the graph. 54

Figure 4–5: Demonstration of the digital averaging noise reduction technique. The voltage distribution of 60

the unaveraged noise record is represented by the Gaussian distribution with the larger standard deviation (82 mV). After 10 averages the standard deviation of the noise voltage distribution decreased to 26 mV. The data points indicated in the figure were obtained by generating a count versus voltage histogram for a 10,000 sample noise voltage record. The lines connecting the data points represent the best–fit Gaussian distributions which were calculated using a weighted least–squares algorithm. The inset of this figure shows 100 point portions of the 10,000 sample noise records used to generate the histogram values. (The data points and best–fit distributions have been normalized so that the areas under each Gaussian distribution are identical.)

Figure 4–6: Demonstration of the relationship between the RMS noise voltage and the number of digital averages. Plotting the logarithm of the RMS noise voltage as a function of the logarithm of the number of digital averages yields the data points indicated on the graph. The solid line represents a linear least–squares approximation to the data points. 61

CHAPTER 1

INTRODUCTION

The advent of commercially–available lead–salt tunable diode lasers (TDL's) in the early 1970's has resulted in widespread use of these lasers for high resolution infrared spectroscopy. TDL–based spectrometers possess several key advantages compared to traditional spectroscopic techniques which employ broad–band lamps in conjunction with dispersive or interferometric instruments. TDL's combine a relatively large output power (typically 100's of μW) with a narrow laser linewidth on the order of 10^{-4} cm^{-1}, resulting in an infrared light source with a high spectral brightness (output power per unit spectral width). This attribute of TDL's provides for both high sensitivity measurements and a spectral resolution limited not by the instrumental broadening typical of traditional spectrometers but rather by the linewidth of the absorbing transition. Through a combination of compositional tuning of the ternary lead–salt alloys and temperature tuning, the lead–salt lasers exhibit almost continuous wavelength tunability in the $3 - 30$ μm wavelength region. Since most molecules possess rovibrational transitions within the infrared spectral region, it is not surprising that lead–salt lasers have become important light sources in both the laboratory and industrial environments.

Historically, TDL's have been exploited in the high sensitivity detection of steady–state infrared absorptions, i.e., absorptions in which the concentration of the absorbing species remains constant or varies slowly in time. Since TDL's have found wide use in high resolution infrared spectroscopy, extensive research has been

undertaken to enhance the sensitivity of TDL–base instrumentation. At present, infrared absorption lines with a line centre absorption of 10^{-4} can be detected on a routine basis. Under optimum conditions, residual noise levels equivalent to a line centre absorption of 10^{-5} can be achieved in gases at low pressure [1]. The combination of high sensitivity and high resolution afforded by tunable diode lasers has been exploited for the detection of atmospheric pollutants and trace gases both in the laboratory and in the stratosphere [1–3]. However, the majority of the detection techniques developed to date are only suitable for the detection of a steady–state absorption. Typically, the detection systems operate with time constants on the order of one second, and consequently cannot monitor fast changes in absorption.

In recent years, there has been increased interest in the use of TDL's to monitor transitions with a line centre absorption which varies with time, i.e., a transient infrared absorption [4–6]. In a laboratory environment, transient species can often be created using either a pulsed laser or a pulsed electric discharge. These species can then be monitored by probing their infrared absorption spectra, provided such measurements can be made on a sufficiently fast time scale.

The temporal resolution of absorptions is an important spectroscopic tool in the areas of chemical reaction kinetics and molecular dynamics. Short–lived species such as free radicals often act as intermediaries in a chemical reaction sequence. These transient species play important roles in such diverse areas as atmospheric and interstellar chemistry, biology and semiconductor materials processing [7]. In order to identify the pertinent intermediate species, one can probe the transient absorption and thus gain a complete understanding of a specific reaction mechanism.

Transient absorption spectroscopy is also an important tool in the study of molecular dynamics. For instance, the relaxation rates of vibrational levels play an important role in the area of excited–gas dynamics. These relaxation rates can be measured by probing the transient absorption spectra of pertinent transitions, and this type of measurement is very important in the study of pulsed and continuous–wave gas laser systems [8].

There are two major considerations needed to evaluate a technique used to monitor the time evolution of an absorption line. Primarily, the technique must provide sufficient detection bandwidth to both capture the absorption event and to provide accurate information regarding the lifetime of the absorption. Since free radicals or molecular ions tend to be extremely reactive, creation of large concentrations of these species is difficult. Thus, the monitoring technique must also be sensitive to small changes in the line centre absorption of the probe transition. For these reasons, a variety of techniques have recently been developed to shorten the response time of TDL instrumentation while retaining the high sensitivity. In particular, direct frequency modulation of lead–salt lasers in conjunction with heterodyne detection [9] and gated–integration techniques [6] have been proposed for the sensitive detection of transient species.

The purpose of this thesis is to describe an alternate technique for monitoring transient infrared absorptions with TDL's. The technique is simpler to implement and yields superior performance when compared with frequency modulation and gated–integration techniques. The technique is essentially a high frequency version of the sweep integration technique pioneered by Jennings [10] and modified by Cassidy and Reid [11]. In terms of measured performance, the detection technique is able to reproducibly achieve near detector–noise–limited

sensitivities in the 1×10^{-5} equivalent absorbance range with an effective response time of one microsecond.

After briefly reviewing some of the important physical characteristics of lead–salt lasers in Chapter 2, the experimental results for both 100 kHz and 500 kHz TDL modulation rates will be presented in Chapter 3. Chapter 4 includes a discussion of noise reduction techniques commonly employed in TDL–based instrumentation. This discussion will include a comparison of bandwidth reduction techniques commonly employed in direct detection absorption measurements, and digital averaging techniques pertinent to the transient absorption monitoring technique described in the body of this thesis. Finally, conclusions and suggested extensions of this work are described in Chapter 5.

CHAPTER 2

GENERAL CHARACTERISTICS OF LEAD–SALT TUNABLE DIODE LASERS

2.1 Introduction

The technique of transient absorption spectroscopy, which forms the basis of this thesis, relies on the use of a lead–salt tunable diode laser as a source of coherent infrared radiation. (Recently, III–V alloy lasers typically used in optical communications have been used to monitor steady–state absorptions [12]. However, transient detection has not yet been attempted.) The purpose of this chapter is to provide a brief introduction to the structure and properties of Pb–salt TDL's. The material considerations involved in the fabrication of TDL's as well as the geometry and properties of the lasing structure will be discussed in Section 2.2. The subsequent section will involve a discussion of the optical frequency tuning characteristics of TDL's. It is the tuning characteristics of Pb–salt lasers which are important to this thesis, since the transient absorption detection technique relies on the ability to modulate the wavelength of the source laser. In Section 2.4, it will be seen that current modulation of the TDL in the vicinity of an absorption line results in a detected signal which consists of an absorption line superimposed upon a background AM component.

2.2 Material Considerations, Structure, and Lasing Properties of TDL's

Lead–salt lasers are fabricated from ternary alloys of the binary

compounds PbTe, PbSe, PbS, and SnTe. These binary compounds all crystallize in the cubic NaCl or rock–salt configuration which explains the derivation of the name lead–salt laser. Figure 2–1 [13] shows the variation of energy gap, lattice constant and refractive constant for the ternary alloys of the lead–salt family. This diagram includes the alloy system $Pb_{1-x}Sn_xSe$, which can only be used to fabricate lasers for lead–rich compounds. Since SnSe crystallizes in an orthorhombic configuration, the lead–salt crystal structure can only be supported for compositions where $x < 0.4$ [13]. The ternary compound $PbTe_{1-x}S_x$ is in fact not a good candidate for laser fabrication. Due to the large difference in the lattice constants of PbTe and PbS, this alloy tends to be very brittle thus making device fabrication impractical.

The lasing action in Pb–salt lasers is a result of stimulated radiative transitions between the conduction and valence bands of the semiconductor material. It is the magnitude of the band–gap, E_g, which primarily determines the emission wavelength. By varying the composition of the ternary alloy system, it can be seen from Fig. 2–1 that lead–salt lasers can be compositionally wavelength–tuned from about 4 μm to over 30 μm. Resonances of several important molecules in this infrared region are shown in Figure 2–2 [14]. (For certain compositions of $Pb_{1-x}Sn_xTe$ and $Pb_{1-x}Sn_xSe$ a zero band–gap condition is reached which promises, in principle, lasing action out to very large wavelengths. Unfortunately, emission wavelengths beyond about 34 μm have not yet been realized.) It should be noted that the laser used for the transient absorption measurements described in this thesis was fabricated from a $Pb_{1-x}Sn_xTe$ alloy with an emission wavelength of about 8 μm.

Figure 2–1: Variation of energy gap (E_g), lattice constant (a) and refractive index (n) as a function of the lead–salt alloy composition at 77K. (Adapted from [13].)

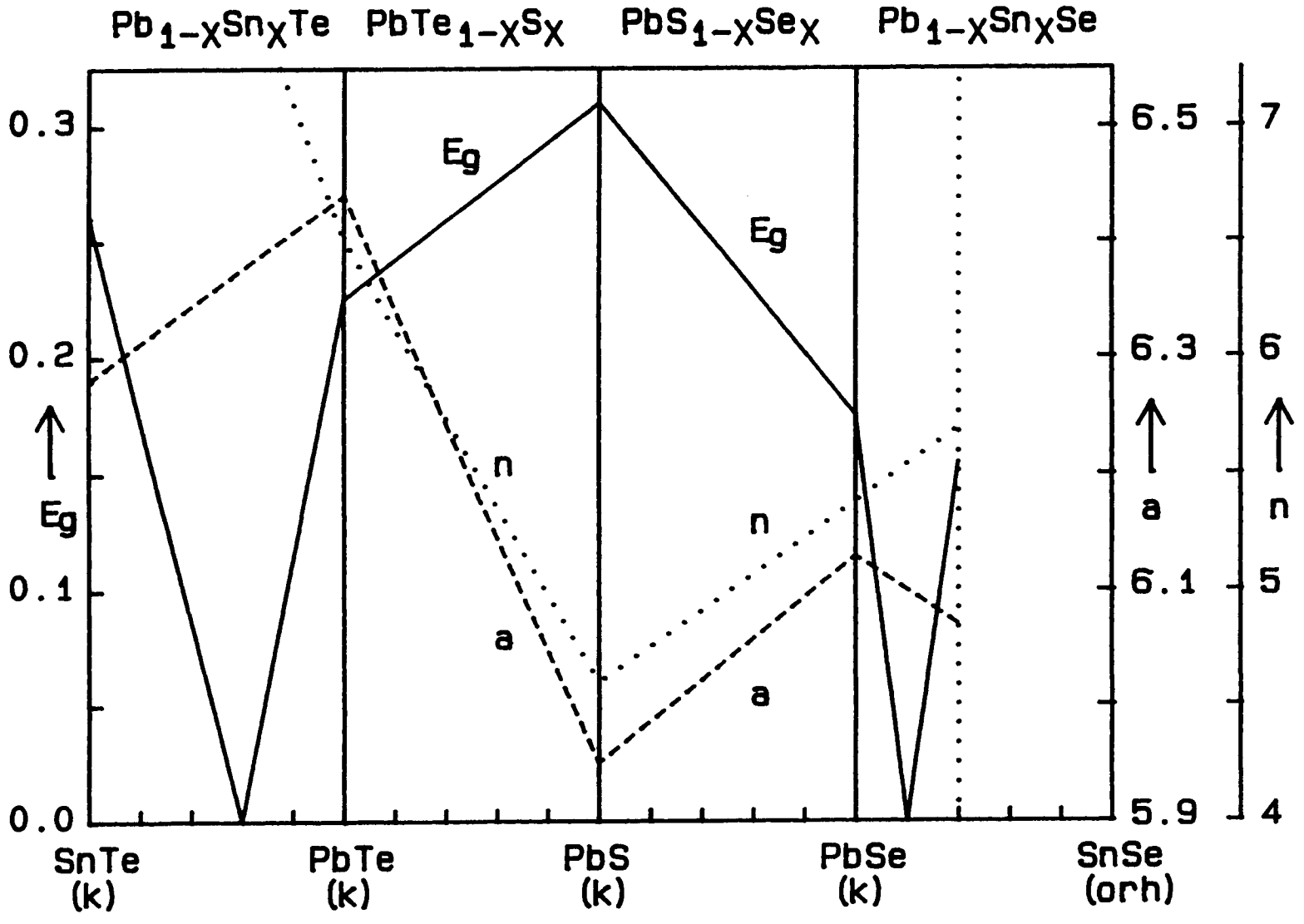
Pb1-XSnXTe
PbTe1-XSX
PbS1-XSeX
Pb1-XSnXSe
0.3
0.2
0.1
0.0
Eg
Eg
Eg
n
a
n
a
6.5
6.3
6.1
5.9
a
7
6
5
4
n
SnTe (k)
PbTe (k)
PbS (k)
PbSe (k)
SnSe (orh)

Figure 2–2: Resonance wavelengths of several important molecules which are often used in infrared spectroscopy. Also indicated are the wavelength regions which can be attained by compositional tuning of several lead–salt laser systems. (Adapted from [14].)

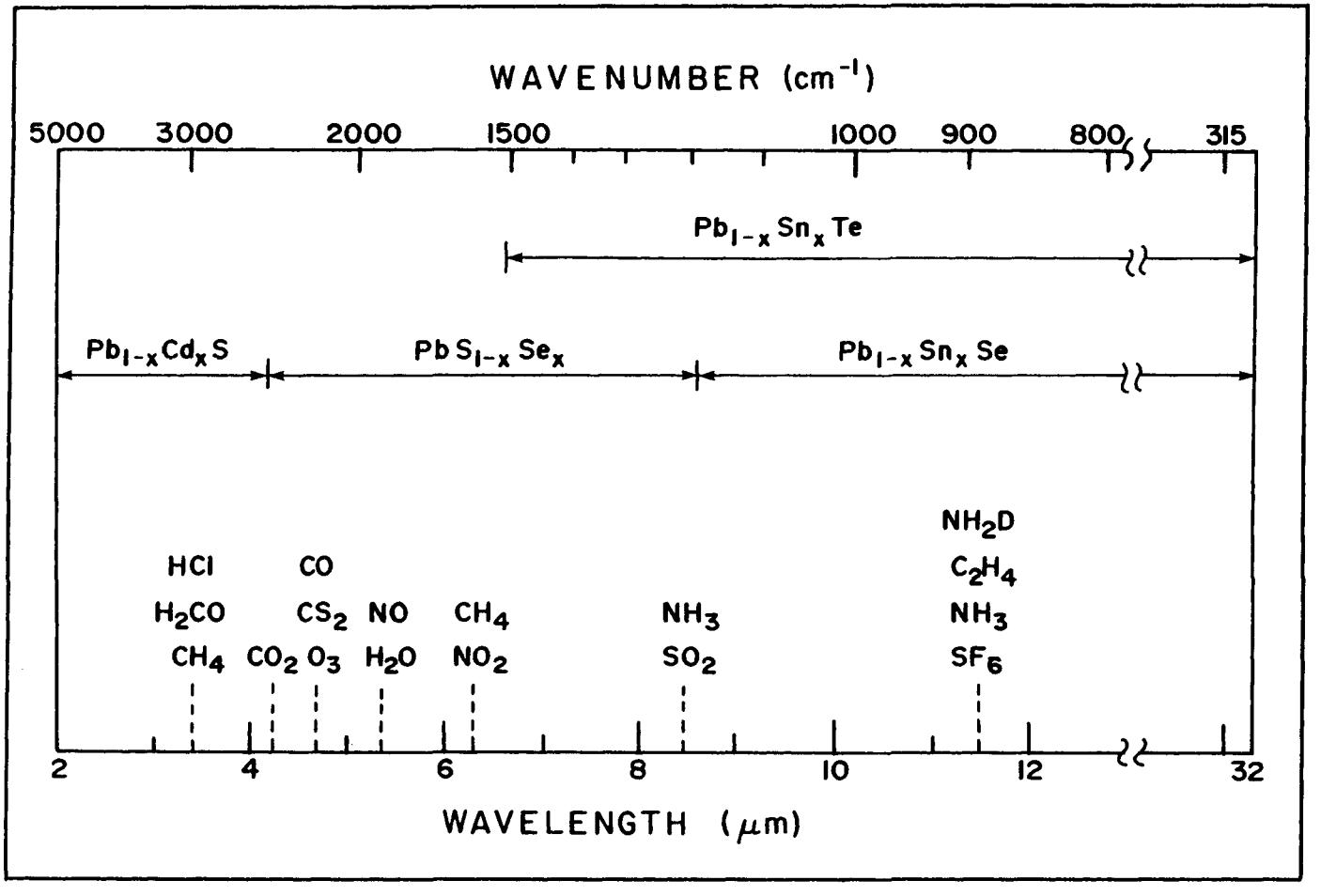
WAVENUMBER (cm⁻¹)
5000
3000
2000
1500
1000
900
800
315
Pb1-x Snx Te
Pb1-x Cdx S
Pb S1-x Sex
Pb1-x Snx Se
HCl
H2CO
CH4
CO
CS2
CO2
O3
NO
H2O
CH4
NO2
NH3
SO2
NH2D
C2H4
NH3
SF6
2
4
6
8
10
12
32
WAVELENGTH (μm)

Figure 2–3 [14] shows a schematic diagram of a typical stripe geometry lead–salt diode laser. The p–n junction of this single heterojunction laser is created using a diffusion process through a stripe geometry mask during fabrication. The end faces are cleaved along natural crystal planes to form a conventional Fabry–Perot laser cavity. Notice that this is a very simple structure compared to those found in optical communications lasers made from the III–V compounds. Typical lead–salt lasers must be operated at cryogenic temperatures (< 77 K) and threshold currents tend to be relatively high (typically 0.4 A). The high threshold currents are due to the fact that the Pb–salt laser structure results in poor optical confinement due to the reliance on the optical gain–guided mechanism. Poor electrical carrier confinement also results from the single heterojunction configuration. On the other hand, optical communications lasers are produced from high quality double–heterostructure configurations which use cladding layers to provide optical index guiding. For these reasons III–V lasers can operate at room temperature with small threshold currents (< 100 mA). From the band–gap, lattice constant and refractive index curves in Fig. 2–1, it seems that double heterostructure, index guided lasers could indeed be constructed from Pb–salt materials, but unfortunately this fabrication technology is still in its infancy.

When the lead–salt laser is current–biased above its threshold value, the output light consists of one or more laser modes with an optical power level on the order of 100's of μW. The separation of these spectral modes is defined by the characteristics of the Fabry–Perot cavity and is typically about 2 cm^{-1} for a 500 μm long device [13]. Variation of appropriate parameters of the laser allows the modes to be shifted in wavelength. This important wavelength tuning capability of the Pb–salt diode laser is the subject of the next section.

Figure 2–3: Schematic diagram of a typical lead–salt diode laser. (Adapted from [14].)

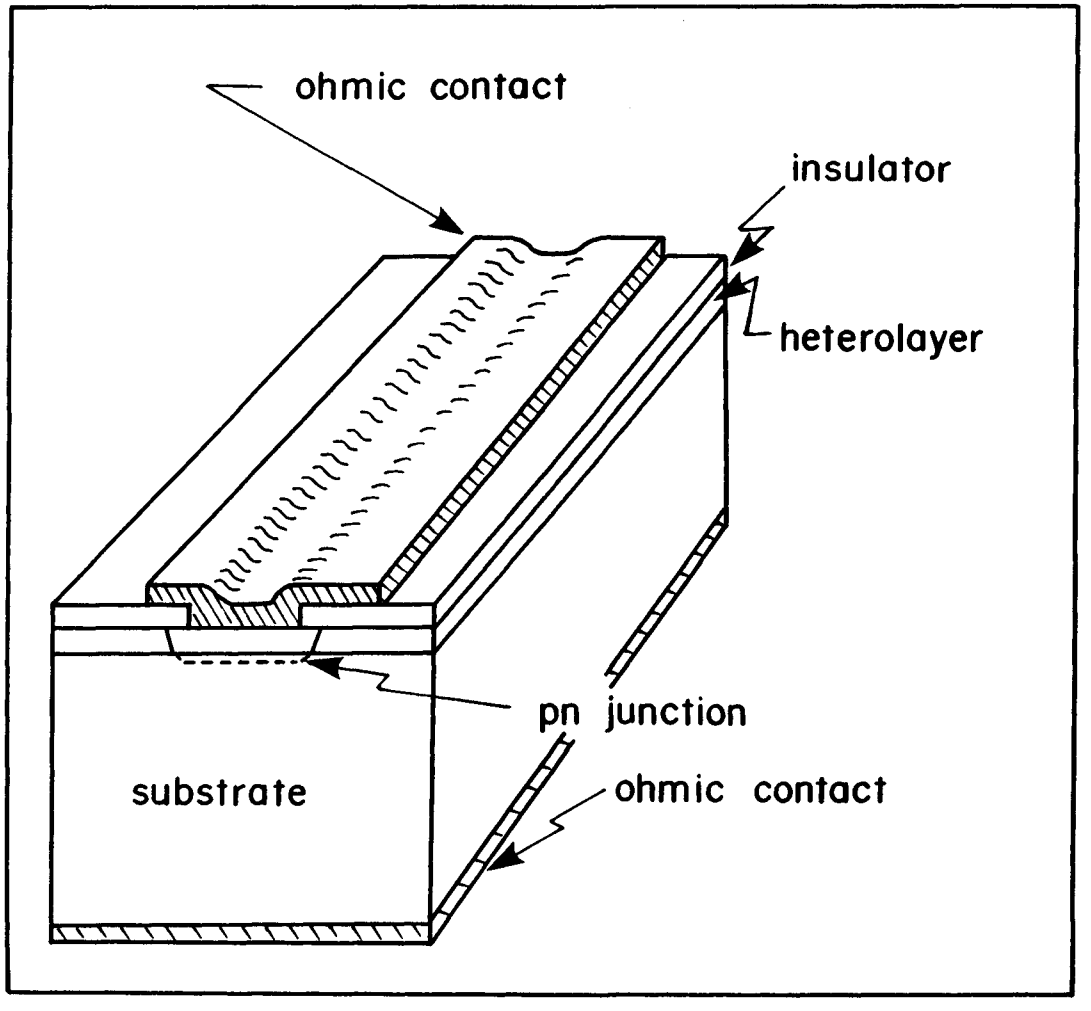
ohmic contact
insulator
heterolayer
pn junction
substrate
ohmic contact

2.3 Wavelength Tuning of TDL's

The wavelength tunability of Pb–salt diode lasers makes these devices ideal light sources for probing infrared absorption spectra. It has already been mentioned that compositional tuning of the material constituents during laser fabrication allows for emission wavelengths within the important 3–30 μm spectral region. This compositional tuning essentially sets the wavelength peak of the laser gain profile. Appropriate adjustment of additional parameters can then be employed to tune this output emission frequency over smaller intervals.

The band–gap and refractive index of Pb–salt lasers are known to vary as a function of hydrostatic pressure, magnetic field and operating temperature [14]. It is the latter parameter, the operating temperature, which is the preferred method for wavelength tuning of commercial Pb–salt lasers. Coarse wavelength tuning is provided by adjusting the ambient temperature of the laser diode which alters the band–gap of the active region material at a rate of about +0.5 meV/K [15]. This coarse tuning typically occurs over a 200 cm^{-1} interval and it is manifested as a series of discrete steps in which the laser emission frequency jumps from one longitudinal mode to the next. This is commonly referred to as a "mode hop". On a finer scale, a given longitudinal mode can be continuously wavelength tuned through a temperature–dependent refractive index effect which alters the optical path length of the Fabry–Perot cavity. This fine wavelength tuning is provided by current injection which results in an ohmic heating effect. Figure 2–4 represents an idealised plot of laser emission frequency as a function of current. Note also from Fig. 2–4 that the extent to which a given laser is single–moded depends upon the degree of overlap of the continuous tuning rate curves at a given bias current.

Figure 2–4: An idealised plot of the laser emission frequency as a function of current. Continuous optical tuning ranges are separated by discrete wavelength jumps known as "mode hops".

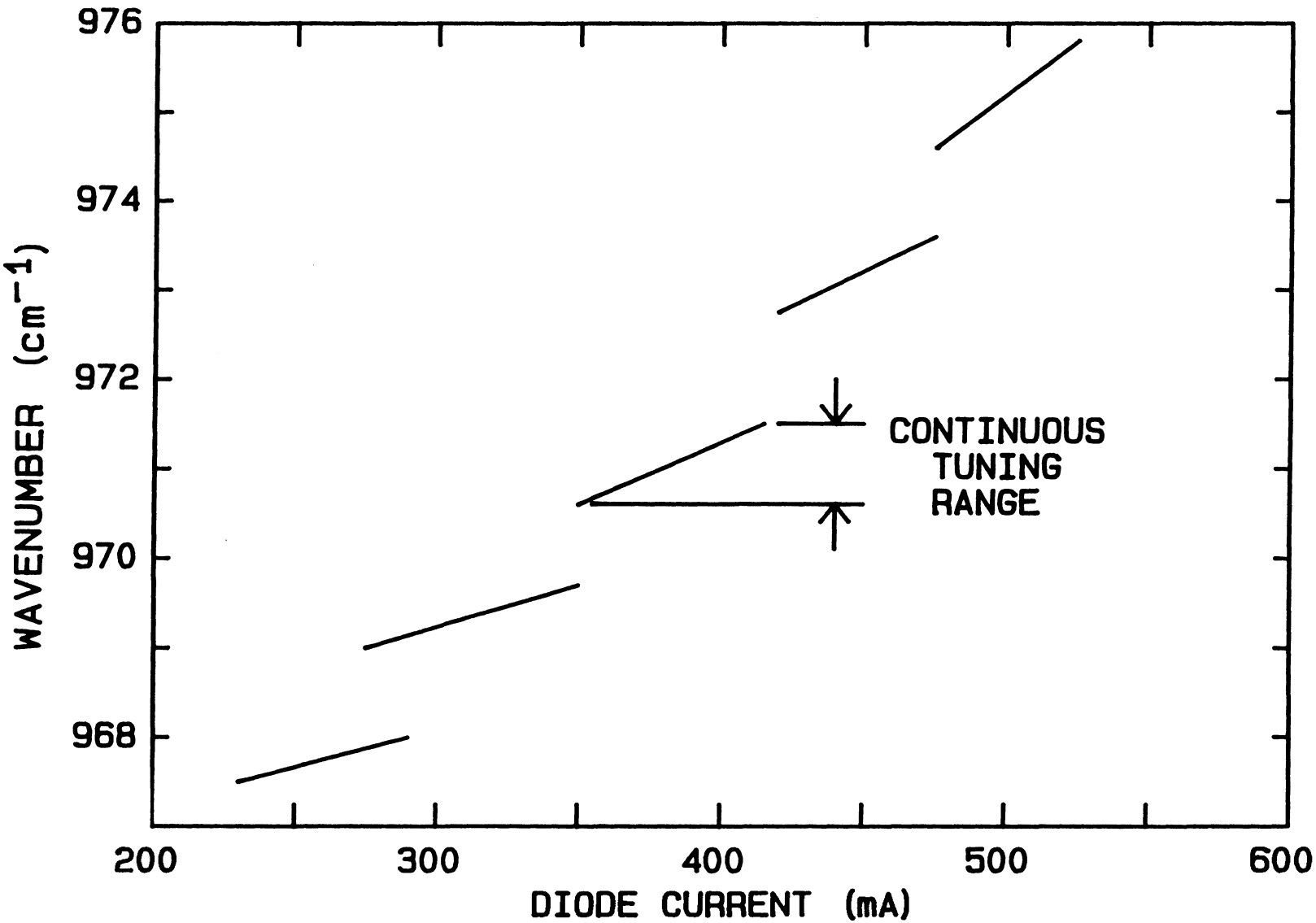
976
974
972
970
968
WAVENUMBER (cm^{-1})
CONTINUOUS
TUNING
RANGE
200
300
400
500
600
DIODE CURRENT (mA)

2.4 Effect of TDL Modulation in the Vicinity of an Absorption Line

Before a discussion of the actual experimental apparatus used to detect transient absorptions is undertaken in the next chapter, it will be useful to first discuss the effect of modulating the TDL wavelength in the vicinity of an absorption line. Figure 2–5 shows a computer–generated plot of transmitted laser power through a low pressure (Doppler–broadened) gas as a function of the TDL optical frequency. This type of plot is commonly generated by mechanically chopping the TDL beam and then using phase–sensitive detection techniques (i.e., a lock–in amplifier) to monitor the transmitted laser power as the bias current supplied to the TDL is slowly ramped upwards. Due to the narrow linewidth of the laser, the Doppler–broadened absorption profile is fully resolved as the TDL emission frequency tunes through the resonant transition.

If the laser emission frequency is tuned to the line centre absorption frequency and a current modulation is applied to the TDL, two important effects are observed at the output of the radiation detector. The detected waveform indicates the effects of both an amplitude modulation and an optical frequency modulation as shown in Figure 2–5. The amplitude modulation effect is caused by the linear relationship between the TDL output power and the applied bias current, whereas the optical frequency modulation is caused by the refractive index effect outlined in the previous section. These two modulation effects result in the absorption line being superimposed upon a background AM component. This AM component typically has a magnitude equivalent to 5–10 % of the total laser power. It should also be noted from Fig. 2–5 that since the TDL wavelength sweeps across the absorption line twice per modulation cycle, the absorption line sampling rate is

Figure 2–5: Idealised plot of the detected optical power as the laser frequency tunes through a Doppler–broadened absorption line. An applied current modulation to the TDL results in a detector signal which consists of both amplitude and optical frequency modulation effects. The resultant detector signal shows the absorption line superimposed upon the background AM component.

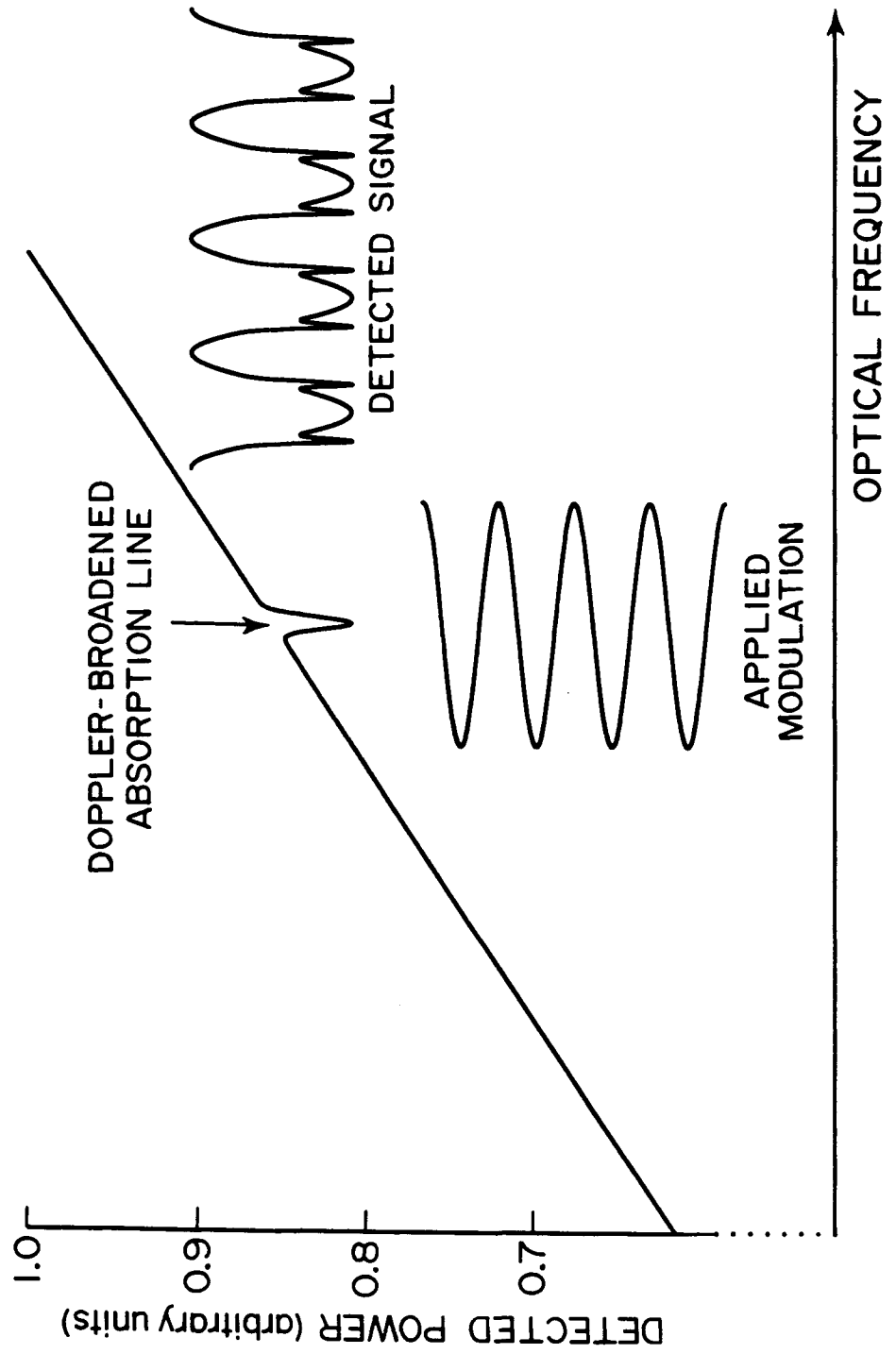
DETECTED POWER (arbitrary units)
1.0
0.9
0.8
0.7
DOPPLER-BROADENED ABSORPTION LINE
DETECTED SIGNAL
APPLIED MODULATION
OPTICAL FREQUENCY

intrinsically twice the TDL modulation rate.

2.5 Summary

In this chapter, some of the important physical properties of lead–salt tunable diode lasers have been reviewed. In particular the mechanisms for wavelength tuning of these infrared laser sources have been briefly outlined. The wavelength tunability of TDL's forms the basis of the transient absorption monitoring technique which will be discussed in the next chapter.

CHAPTER 3

HIGH SENSITIVITY DETECTION OF TRANSIENT INFRARED ABSORPTIONS

3.1 Introduction

Recently, there has been increased interest in the use of TDL's to monitor transient infrared absorptions. There are many applications where the concentration of an infrared–active constituent of a gas changes concentration on a short time scale [7]. Transient species can be monitored using lead–salt lasers provided such measurements can be made on a sufficiently fast time scale. A variety of techniques have been proposed for the fast response time, high sensitivity detection of transient infrared absorptions. These techniques include FM–heterodyne [9] and gated–integration [6] techniques.

It is the purpose of this chapter to describe an alternative technique for monitoring transient infrared absorptions, which has several advantages compared to other techniques. Initial results describing an application of this technique for the detection of CF_2 were given in a publication by Beckwith et al [16]. The transient absorption detection technique has since been refined and the response time has been considerably shortened. Beckwith et al. were able to monitor transient absorptions using a TDL modulation rate of 100 kHz. An appropriate modification to the TDL control circuitry has since extended the frequency response of the modulation circuitry into the MHz regime. Thus the present technique has the ability to reproducibly achieve sensitivities limited primarily by detector noise

at the $\sim 1 \times 10^{-5}$ equivalent absorbance level with microsecond response times.

In the next section, the experimental apparatus for the creation and monitoring of transient infrared absorptions is described. Included is a description of the modification to the TDL control circuitry required to ensure high TDL modulation rates. Transient absorption results for both 100 kHz and 500 kHz TDL modulation rates are documented in Section 3.3 and Section 3.4 respectively. A discussion of the sensitivity of the detection technique is provided in Section 3.5.

3.2 Experimental Apparatus

Figure 3–1 is a schematic diagram of the experimental apparatus for the creation and monitoring of transient infrared absorptions. The collimated TDL beam passes through a 75 cm long, 3 cm inner–diameter discharge tube. The laser beam is subsequently focused onto a HgCdTe detector using a Ge lens. The discharge tube was equipped with NaCl Brewster windows to ensure maximum throughput of the polarized laser beam. To minimize the deleterious effects of optical feedback into the TDL caused by reflections, the detector was tilted at an angle of approximately 30 degrees with respect to the optical axis. The TDL used in the experiment could be tuned from approximately 1200 cm^{-1} to 1400 cm^{-1} and was fabricated from the $Pb_{1-x}Sn_xTe$ ternary alloy system. The function of the other apparatus depicted in Fig. 3–1 will become evident later in this chapter.

The TDL control electronics shown in Fig. 3–1 were supplied by Laser Analytics Inc. The purpose of these electronics was to stabilize the operating temperature of the cryogenically–cooled laser diode and to provide a stable bias current to the device. Normally, the control electronics allow for TDL current

Figure 3–1: Schematic diagram of the apparatus used for the creation and monitoring of transient absorptions. The discharge tube contains a flowing mixture of N_2O in He at a total pressure of approximately 10 Torr. The discharge current is pulsed at a repetition frequency of 10 Hz. Each current pulse lasts for 200 μs and has a peak current of 250 mA.

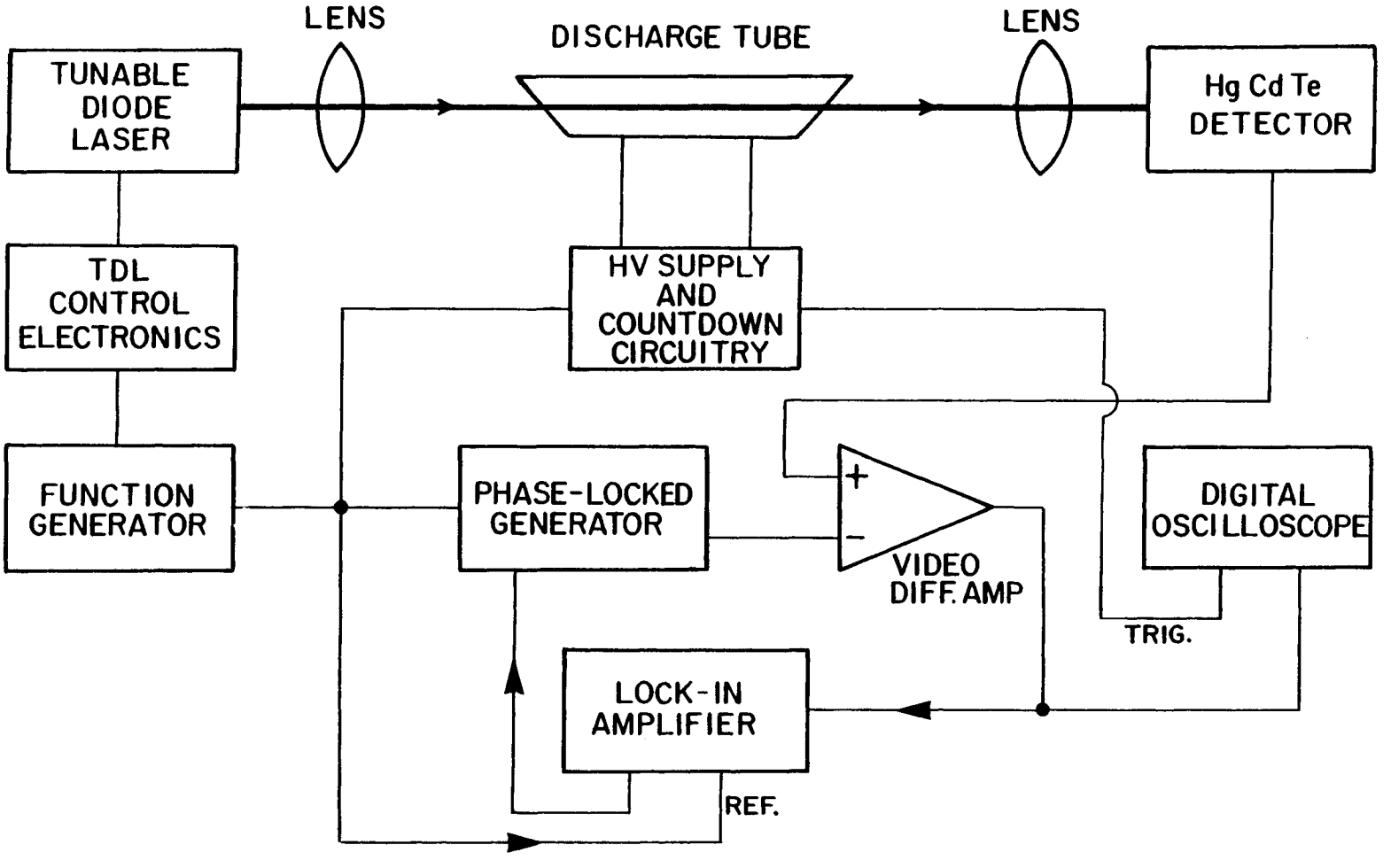
LENS
DISCHARGE TUBE
LENS
TUNABLE DIODE LASER
Hg Cd Te DETECTOR
TDL CONTROL ELECTRONICS
HV SUPPLY AND COUNTDOWN CIRCUITRY
FUNCTION GENERATOR
PHASE-LOCKED GENERATOR
+
−
VIDEO DIFF. AMP
DIGITAL OSCILLOSCOPE
TRIG.
LOCK-IN AMPLIFIER
REF.

modulation rates of less than 10 kHz. To attain the high modulation rates required to implement the transient absorption detection technique, the existing modulation electronics were bypassed with the addition of a bias–T insertion circuit. The schematic diagram and frequency response for the bias–T insertion circuit are shown in Figure 3–2. The essential elements of this circuit are the 1 μF DC blocking capacitor and the 40 μH inductor. The purpose of the inductor is to allow unimpeded passage of the DC laser bias current while simultaneously providing a blocking impedance for the AC modulation current. The 51 Ω resistor was inserted to provide a matched termination impedance for a 50 Ω output–impedance voltage generator. This generator provides the modulation signal to the laser diode. The frequency response curve of the bias–T network shows an approximately flat response from 0 to 10 MHz, with an insertion loss of about 30 dB at 1 MHz. This loss is a result of a voltage divider network which occurs when the laser diode is attached to the output of the bias–T circuit. The frequency response curve shown in Figure 3–2 was actually measured across a simulated laser diode which consisted of a 1 Ω resistor in series with a silicon diode. Simple voltage divider theory predicts an insertion loss of ~34 dB which is comparable to the measured loss. The slight decrease in insertion loss with increasing frequency is probably due to a parasitic shunt capacitance in parallel with the 51 Ω resistance which effectively reduces this resistance at higher modulation frequencies.

With the control electronics modified to allow for high TDL modulation rates, the demonstration of the detection technique required a reproducible and controlled method of generating a transient absorption line in the 1200–1400 cm^{-1} region. The absorption spectrum of N_2O in the 1300 cm^{-1} region is very well known [17], and an electric discharge can be used to place a significant population

Figure 3–2: Schematic diagram and frequency response of the bias–T insertion circuit. This circuit allows a DC bias current and an AC modulation signal to be combined and subsequently applied to the diode laser. The frequency response curve is measured at the output of the bias–T circuit across a simulated laser diode consisting of a 1 Ω resistor in series with a silicon diode.

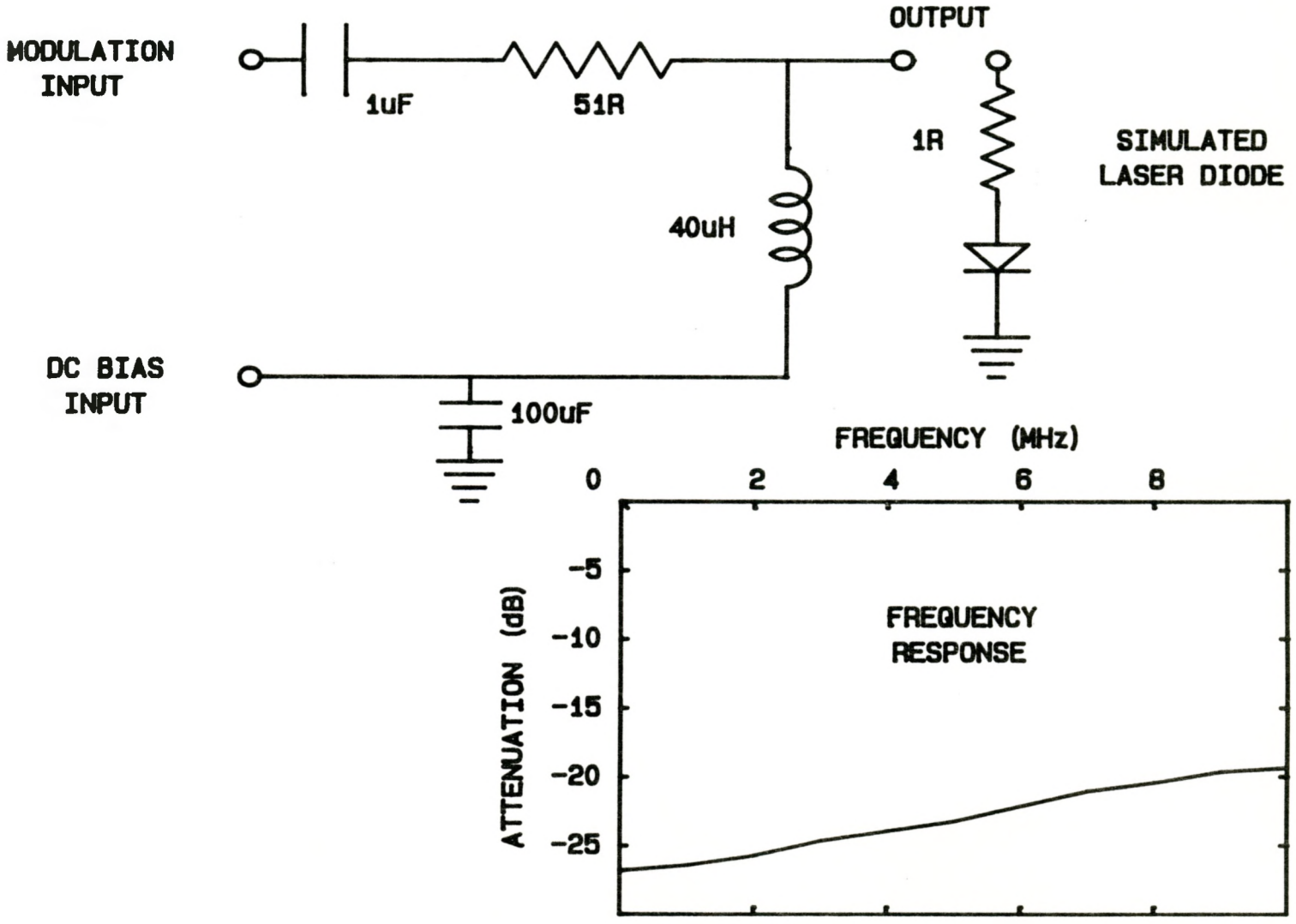
MODULATION INPUT
1uF
51R
OUTPUT
1R
SIMULATED LASER DIODE
40uH
DC BIAS INPUT
100uF
FREQUENCY (MHz)
0
2
4
6
8
ATTENUATION (dB)
-5
-10
-15
-20
-25
FREQUENCY RESPONSE

into the ν_3 vibrational mode of N_2O. (This excitation process is the basis of the 10 μm N_2O laser [18].) Consequently, a low pressure (~10 Torr) flowing mixture of N_2O in a He buffer gas was employed in a pulsed discharge cell configuration to provide well–defined transient absorptions. By varying the concentration of N_2O in the gas mixture, the magnitude of the transient absorption signal could easily be controlled.

The discharge current pulse applied to the cell was created by charging a capacitive network with the high voltage power supply shown in Fig. 3–1. This capacitive network was then discharged through the cell at a repetition frequency of 10 Hz. The 10 Hz clocking waveform was derived from the synchronization signal of the TDL modulation generator using a flip–flop–based divide–by–N circuit. (The 10 Hz signal was also used to provide a reliable trigger to the digital oscilloscope. This ensured that the triggering of the oscilloscope and the firing of the discharge were well synchronized.)

Figure 3–3 shows a conventional direct detection scan of room–temperature N_2O in the 1273 cm^{-1} region. This trace was obtained by mechanically chopping the TDL beam and then using phase–sensitive detection techniques to monitor the transmitted laser power as a function of TDL bias current. The TDL was operating in a single mode within this spectral region with approximately 100 μW of optical power incident upon the detector. The positions of the optical frequencies labelled on the abscissa of Fig. 3–3 were calibrated using N_2O reference lines [17], and a germanium etalon with a well–known fringe spacing (0.01627 cm^{-1}) to provide a relative frequency scale. The inset of Fig. 3–3 indicates the transitions which create the steady–state absorption line marked "L", and the transition responsible for a transient absorption at a calculated frequency of

Figure 3–3: Conventional TDL scan of room temperature N_2O. The line marked "L" has a line–centre absorption of 1.6 %. Also shown in the inset is an energy level diagram of the N_2O molecule indicating the transitions relevant to the experiment. Line "L" is the R(35) line of the $(00^0 0 - 10^0 0)$ band of $^{14}N_2{}^{18}O$. The electric discharge places a transient population in level $02^0 1$, and this population creates a transient absorption on the P(8) transition of the $(02^0 1 - 12^0 1)$ band of $^{14}N_2{}^{16}O$ at 1273.527 cm^{-1}.

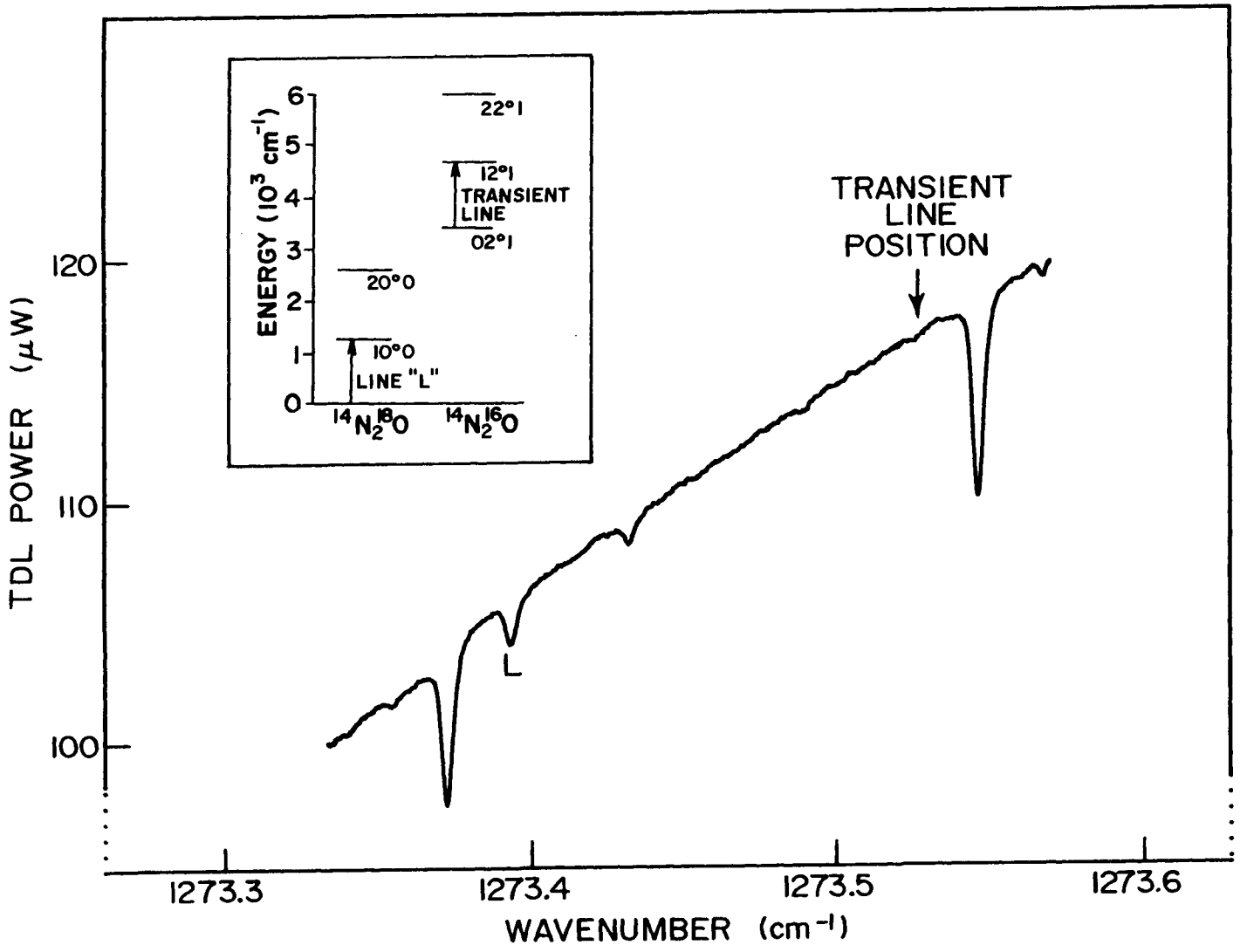
ENERGY (10^3 cm^{-1})
6
5
4
3
2
1
0
22°1
12°1
TRANSIENT LINE
02°1
20°0
10°0
LINE "L"
$^{14}N_2^{18}O$
$^{14}N_2^{16}O$
TRANSIENT LINE POSITION
L
TDL POWER (μW)
120
110
100
1273.3
1273.4
1273.5
1273.6
WAVENUMBER (cm^{-1})

1273.527 cm^{-1}.

When a current modulation is applied to the TDL, the detector output signal consists of both an optical frequency modulation and an amplitude modulation effect. These two modulation effects were discussed in Section 2.4. If the laser is biased so that the TDL wavelength is in the vicinity of an absorption line, the applied current modulation results in the idealised detector signal shown in the upper left portion of Figure 3–4. Both modulation effects are evident in this idealised signal which shows the absorption line superimposed upon the AM background component.

The AM component shown in Fig. 3–4 typically has a magnitude equivalent to approximately 10 % of the total laser power, but this component contains no useful absorption information. In order to allow for digital processing of waveforms, a digital oscilloscope is often used as a storage element. Owing to its large magnitude, the amplitude modulation component causes problems when trying to detect absorptions in the 10^{-4} to 10^{-5} equivalent absorbance range. This is due to the limited dynamic range of digital oscilloscopes – an 8–bit analog–to–digital converter gives a resolution of 1 part in 256. Thus, an absorption smaller than $1{\times}10^{-4}$ would be difficult to detect due to the presence of quantization noise for an AM component which has a magnitude equivalent to 10 % of the total TDL optical power.

To fully utilize the dynamic range of the digital oscilloscope, it is necessary to remove at least the fundamental frequency component which dominates the AM background signal, *before* digitization. This can be accomplished using a variety of techniques including band–reject filtering and analog subtraction. Fig. 3–4 shows an idealized schematic of the analog subtraction technique which is used

Figure 3–4: Idealised schematic which shows the technique of analog subtraction. The detector signal consisting of an absorption line superimposed upon an AM background component is combined with a sine wave at the inputs of a differential amplifier. Proper adjustment of the phase and amplitude of the sine wave from the phase–locked generator ideally results in an output signal which solely consists of the absorption signal.

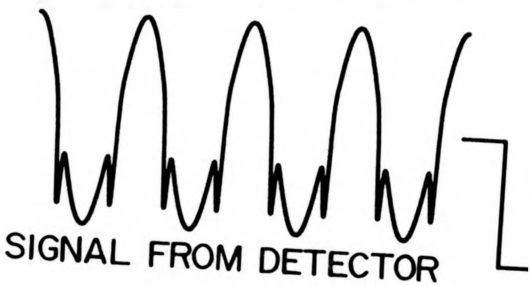
SIGNAL FROM DETECTOR

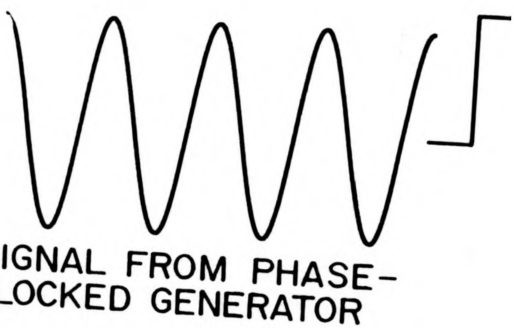
SIGNAL FROM PHASE-
LOCKED GENERATOR

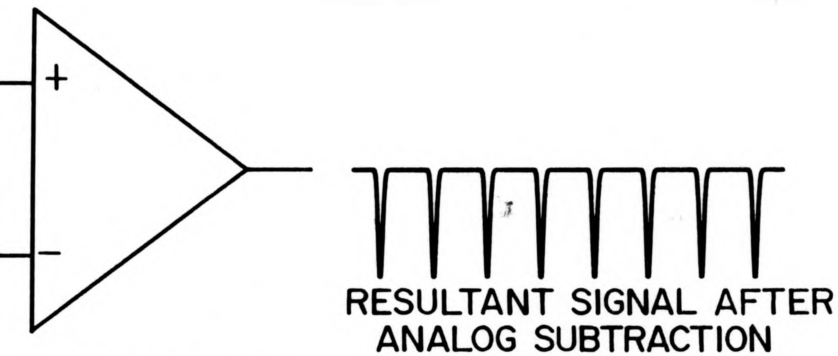

DIFFERENTIAL
AMPLIFIER

in the present work for the transient absorption detection technique. The detector signal composed of the absorption line superimposed upon the background AM component is used as one input to a differential amplifier. The other input signal consists of a sine wave which is to be subtracted from the detector signal. Through an appropriate adjustment of the amplitude and phase of the sine wave, the output of the differential amplifier ideally consists of only the absorption signal shown in Fig. 3–4. (Note that the analog subtraction technique only reduces the fundamental frequency component of the detector signal. Other harmonic components will still be present at the output of the differential amplifier.)

The sine wave used for subtraction purposes can be derived from a number of sources. For low TDL modulation frequencies, the approach adopted by Beckwith et al. [16] was to use variable gain and phase shift circuits which operate on a signal derived from the TDL modulation generator. At higher TDL modulation rates the design of an adjustable phase shift circuit is not trivial. Thus, a different approach was adopted for the present work. A WAVETEK (Model Number 186) phase–lock generator (shown schematically in Fig. 3–1) was synchronized to the TDL modulation frequency. It was found that this generator was able to provide the required gain and phase–shift adjustments necessary to implement the analog subtraction technique.

A practical example of the analog subtraction technique is indicated in Figure 3–5. The first trace shows the result of wavelength modulating the TDL at a frequency of 100 kHz in the vicinity of the absorption line marked "L" in Fig. 3–2. The bottom trace of Fig. 3–5 shows the result of the analog subtraction technique in which the waveform is obtained from the output of an MC1733 video differential amplifier. This trace clearly shows the resultant, well–resolved absorption line.

Figure 3–5: Result of modulating the TDL at 100 kHz across line "L" of Fig. 3–3. Trace A is the output from the HgCdTe detector. The N_2O absorption line is seen superimposed on the sinusoidal AM background signal and is displayed twice per modulation cycle. The lower trace shows the resultant signal after analog subtraction. The differential lineshape is the result of a high pass filter on the input of the video differential amplifier.

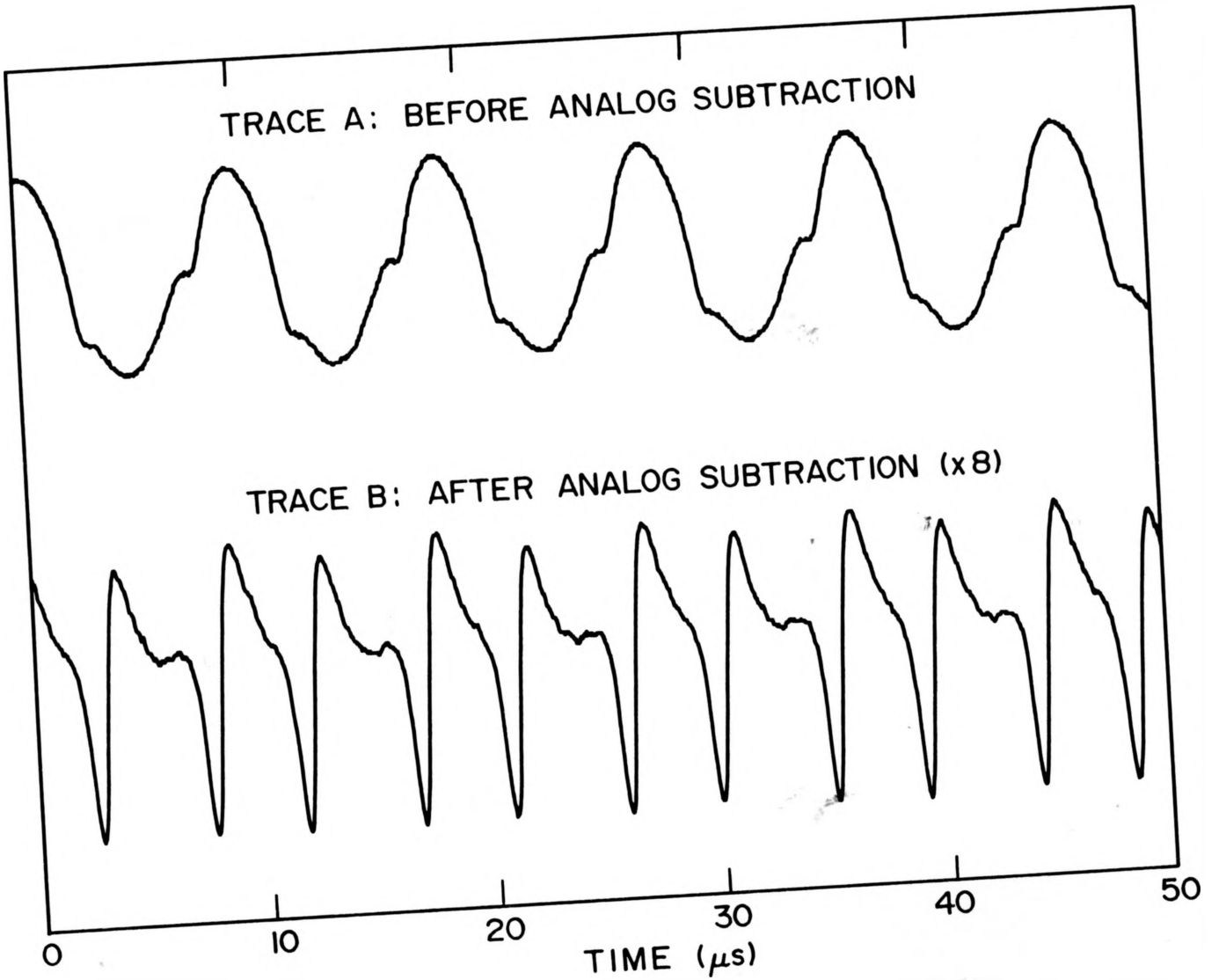
TRACE A: BEFORE ANALOG SUBTRACTION
TRACE B: AFTER ANALOG SUBTRACTION (x8)
0
10
20
30
40
50
TIME (μs)

The slight differential lineshape is caused by a high–pass RC filter network at the input of the differential amplifier. Records of this type can be stored and averaged using the digital oscilloscope to reduce the effects of random noise sources.

The accumulation of steady–state absorption line waveforms such as that shown in the bottom trace of Fig. 3–4 serves an important purpose. Relating the absorption line magnitude in volts (obtained from the oscilloscope display) to the percentage absorption obtained from the direct scan of Fig. 3–3 allows the calculation of a calibrated equivalent absorbance scale.

3.3 Transient Absorption Results for 100 kHz TDL Modulation Rates

The experimental apparatus shown schematically in Fig. 3–1 and discussed in the previous section allowed for the monitoring of a transient infrared absorption in an N_2O discharge. Figure 3–6 illustrates the results of the transient spectroscopy technique for a 100 kHz modulation signal superimposed upon the TDL current. With the pulsed discharge in operation, Trace A was obtained by averaging 1000 digitized records after analog subtraction. The 10 Hz trigger signal provided to the digital oscilloscope was derived from the countdown circuitry which pulses the discharge.

The dominant feature in Trace A is a residual second harmonic component at 200 kHz with an amplitude equivalent to 6×10^{-4} of the total TDL power. Note that the transient absorption signal present in Trace A is not yet clearly resolved and further signal processing techniques are required to retrieve the desired signal. A second trace recorded with the discharge switched off allows the interfering background signals to be reduced. The 200 kHz component is reproduced

Figure 3–6: Demonstration of the high sensitivity transient detection technique for a 100 kHz TDL modulation rate. The TDL is tuned near the $(02^{0}1 - 12^{0}1)$ P(8) transition. Transient absorption is created on this transition by the discharge current pulse which starts at the time indicated by the dashed line. Each trace is the average of 1000 individual scans recorded by the digital oscilloscope. Trace A is recorded with the discharge firing and Trace B is recorded without exciting the discharge. Upon digital subtraction, the lower trace displays the weak absorption line increasing in strength as the current populates the $02^{0}1$ level.

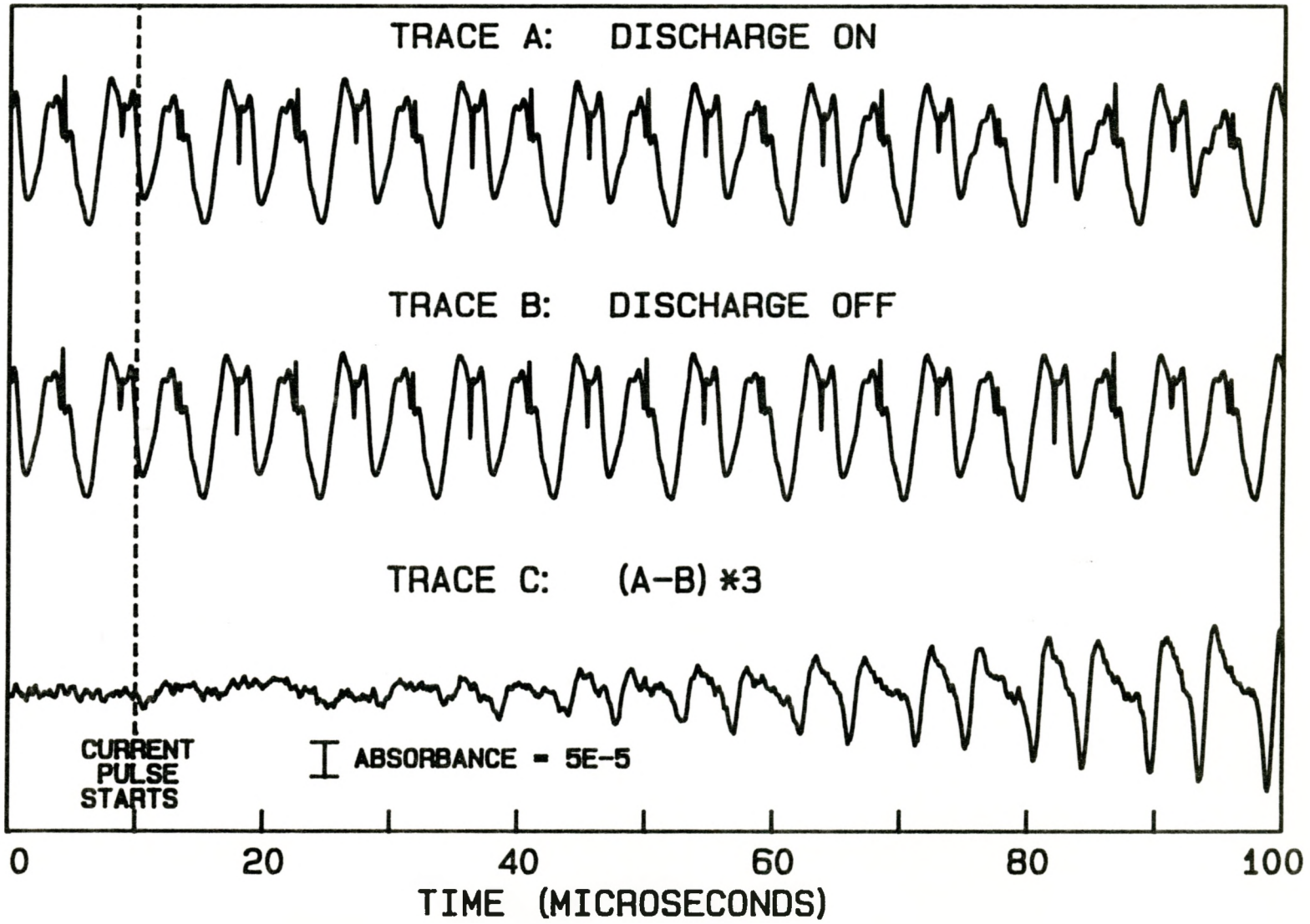
TRACE A: DISCHARGE ON
TRACE B: DISCHARGE OFF
TRACE C: (A-B) *3
CURRENT PULSE STARTS
ABSORBANCE = 5E-5
0
20
40
60
80
100
TIME (MICROSECONDS)

in this second record as are all other harmonic distortions, optical fringes and steady–state absorption lines. The resultant digital subtraction shown in the lower trace of Fig. 3–6 leaves only those features which change between the two records, i.e., the induced transient absorption. This transient absorption is now well–resolved, and it can be seen that the weak absorption line increases in strength as the current pulse populates the lower level of the transition ($02^{0}1$ level in Fig. 3–3). Due to the nature of the wavelength sweep provided by the TDL current modulation, the entire absorption profile is resolved by this technique. Thus, transient linewidth measurements could be performed if required.

Figure 3–7 demonstrates the near detector–noise–limited sensitivity of the detection technique. The first half of the record in Trace B was obtained by removing the N_2O from the discharge tube and then processing the data in a fashion identical to that used to obtain the transient signal reproduced in Trace A. The resultant RMS noise level is equivalent to an absorption of approximately 7×10^{-6} and is dominated by detector noise (depicted in the second half of Trace B). The modulation frequency of 100 kHz allows the recording of the absorption lineshape once every 5 μs. Thus the detection technique can monitor infrared absorptions which change on this timescale with a fractional absorption sensitivity of $\sim 10^{-5}$.

The results depicted in Figure 3–6 clearly indicate the importance of the digital subtraction step for resolving small transient absorptions. The effectiveness of the digital subtraction relies on the fact that the only feature which is different between the two records is the transient absorption signal. An earlier version of the experimental of apparatus did not incorporate the lock–in amplifier shown in Figure 3–1 [16]. Consequently, it was found that after digital subtraction, the resultant

Figure 3–7: Demonstration of the near detector–noise limited sensitivity of the transient absorption detection technique for a 100 kHz TDL modulation rate. Trace A is reproduced from Fig. 3–6 and shows the detection of a transient infrared absorption. The first half of Trace B shows the limiting noise level inherent in the experiment whereas the second half of the trace shows the intrinsic detector noise for comparison purposes. If the lock–in amplifier is not used to track small TDL power variations, Trace C indicates that the noise after the analog and digital subtraction steps consists of an unwanted 100 kHz component. This "fundamental feedthrough" component has a magnitude equivalent to 8×10^{-3} % of the total TDL optical power.

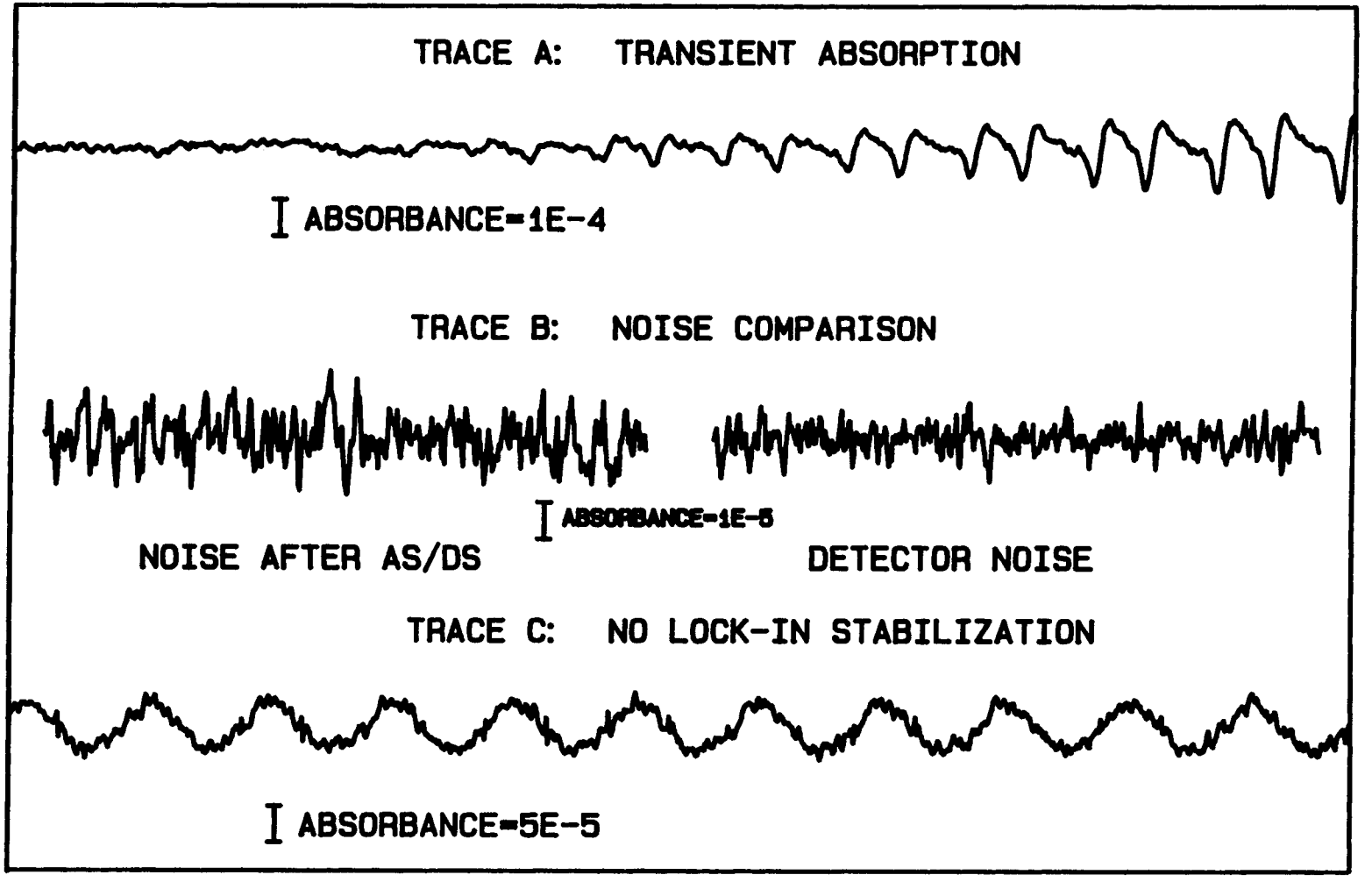
TRACE A: TRANSIENT ABSORPTION
ABSORBANCE=1E-4
TRACE B: NOISE COMPARISON
ABSORBANCE=1E-5
NOISE AFTER AS/DS
DETECTOR NOISE
TRACE C: NO LOCK-IN STABILIZATION
ABSORBANCE=5E-5

record contained a significant component at the fundamental modulation frequency of 100 kHz. This "fundamental feedthrough" signal is shown in Trace C of Figure 3–7 and is caused by minor variations in the TDL power during the time required to capture the two records which are to be digitally subtracted. Since the amplitude modulation on the TDL power is typically 10 %, it is clear that the 100 kHz component resulting from minor power variations at the detector would make it difficult to resolve small transient absorption signals.

It is the function of the lock–in amplifier shown in Fig. 3–1 to track any fluctuations in the detected power of the tunable diode laser. Referencing the lock–in amplifier to the 100 kHz modulation frequency resulted in a DC voltage proportional to any residual fundamental component observed after the differential amplifier. This DC error voltage is then used in conjunction with the voltage controlled amplitude feature of the phase–locked generator to automatically compensate for fluctuations in the detected TDL power. This automatic gain control loop allows for reproducible detector–noise–limited sensitivities in the 10^{-5} equivalent absorbance range, and also allows the circuit to automatically track changes in the TDL output power as the TDL is current tuned to other wavelength regions.

3.4 Transient Absorption Results for 500 kHz TDL Modulation Rates

To achieve absorption sampling rates of 1 MHz, the TDL current modulation frequency was increased to 500 kHz. Due to electronic bandwidth limitations of the lock–in amplifier, the automatic gain control loop could not be utilised at this modulation rate. It was thus anticipated that drifts in the detected

TDL power would result in a significant fundamental harmonic component after the digital subtraction step. Nevertheless, it will be seen that using post–processing techniques, the ultimate sensitivity of the transient detection technique at 500 kHz approaches that dictated by detector noise limitations.

Figure 3–8 illustrates the results of the transient absorption detection technique at the 500 kHz TDL modulation rate. Traces A, B and C were obtained in a fashion similar to those displayed in Figure 3–6, but the lock–in amplifier was not used to null the 500 kHz fundamental component. Consequently, Trace C contains both the absorption signal of interest and an unwanted 500kHz component.

Fortunately, the unwanted 500 kHz component can be removed by Fourier transform filtering, as the absorption signal is only present at frequencies of 1 MHz and above. Trace C was transformed to the frequency domain using standard FFT techniques. The real and imaginary components of the Fourier transform are shown in Figure 3–9. The required filtering was performed by setting those frequency components less than about 800 kHz equal to zero. The bottom trace in Figure 3–9 shows the filtered signal upon returning to the time domain via an inverse Fourier transformation. The transient absorption is now clearly resolved, with the absorption line displayed once every microsecond.

Figure 3–10 shows that the sensitivity of the transient absorption detection technique for the 500 kHz TDL modulation rate approaches that dictated by detector noise limitations. The first half of the record in Trace B was obtained by removing the N_2O from the discharge tube and then processing the record in a fashion identical to that used to obtain the transient signal reproduced in Trace A. The resultant RMS noise level is equivalent to an absorption of approximately 1×10^{-5} which is less than a factor of two larger than the detector noise.

Figure 3–8: Demonstration of the high sensitivity transient absorption detection technique for a 500 kHz TDL modulation rate. After digital subtraction of the records A and B, the resultant signal shown in Trace C reveals the transient absorption superimposed upon a 500 kHz component. This fundamental frequency component is caused by TDL power variations during the time it takes to capture the records which are to be digitally subtracted.

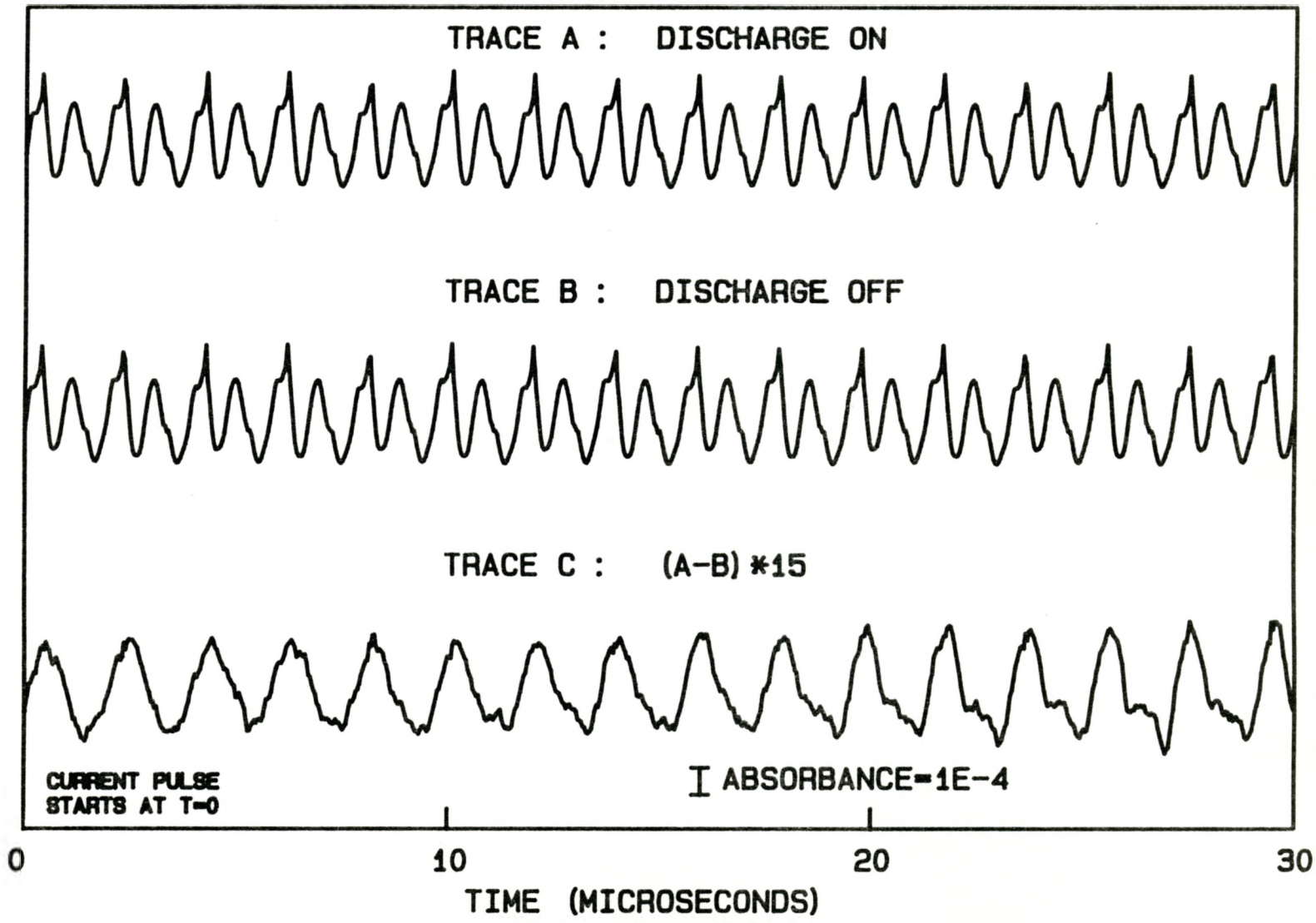
TRACE A : DISCHARGE ON
TRACE B : DISCHARGE OFF
TRACE C : (A-B) *15
CURRENT PULSE
STARTS AT T=0
I ABSORBANCE=1E-4
0
10
20
30
TIME (MICROSECONDS)

Figure 3–9: Removal of the fundamental component using digital filtering techniques. Trace A is reproduced from Fig. 3–8 and shows the transient absorption line superimposed upon the unwanted 500 kHz component. Transforming to the frequency domain using standard FFT techniques produces the real and imaginary frequency component shown in Trace B. Retaining only those frequency components between the filter bars (800 kHz to 3 MHz) results in digital filtering of the original waveform. Returning to the time domain via an additional Fourier transform reveals the well–resolved transient absorption shown in Trace C.

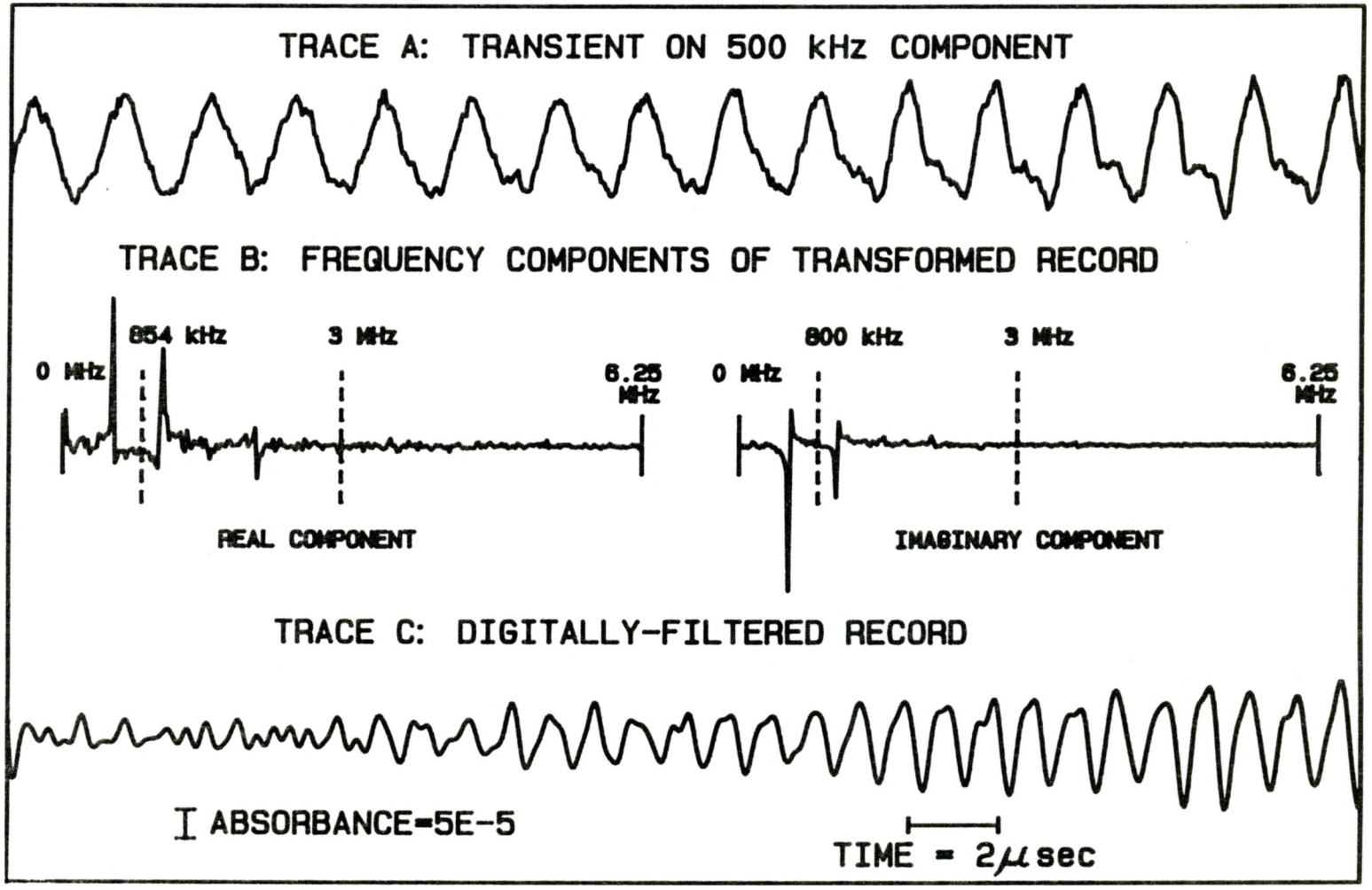
TRACE A: TRANSIENT ON 500 kHz COMPONENT
TRACE B: FREQUENCY COMPONENTS OF TRANSFORMED RECORD
0 MHz
854 kHz
3 MHz
6.25 MHz
REAL COMPONENT
0 MHz
800 kHz
3 MHz
6.25 MHz
IMAGINARY COMPONENT
TRACE C: DIGITALLY-FILTERED RECORD
I ABSORBANCE=5E-5
TIME = 2μsec

Figure 3–10: Demonstration of the near detector–noise limited sensitivity of the transient absorption detection technique. Trace A is reproduced from Fig. 3–9 and shows the detection of a transient absorption at the 500 kHz TDL modulation rate. The first half of Trace B indicates the limiting noise level inherent in the experiment after analog subtraction, digital subtraction and digital filtering. The second half of Trace B shows the intrinsic detector noise for comparison purposes.

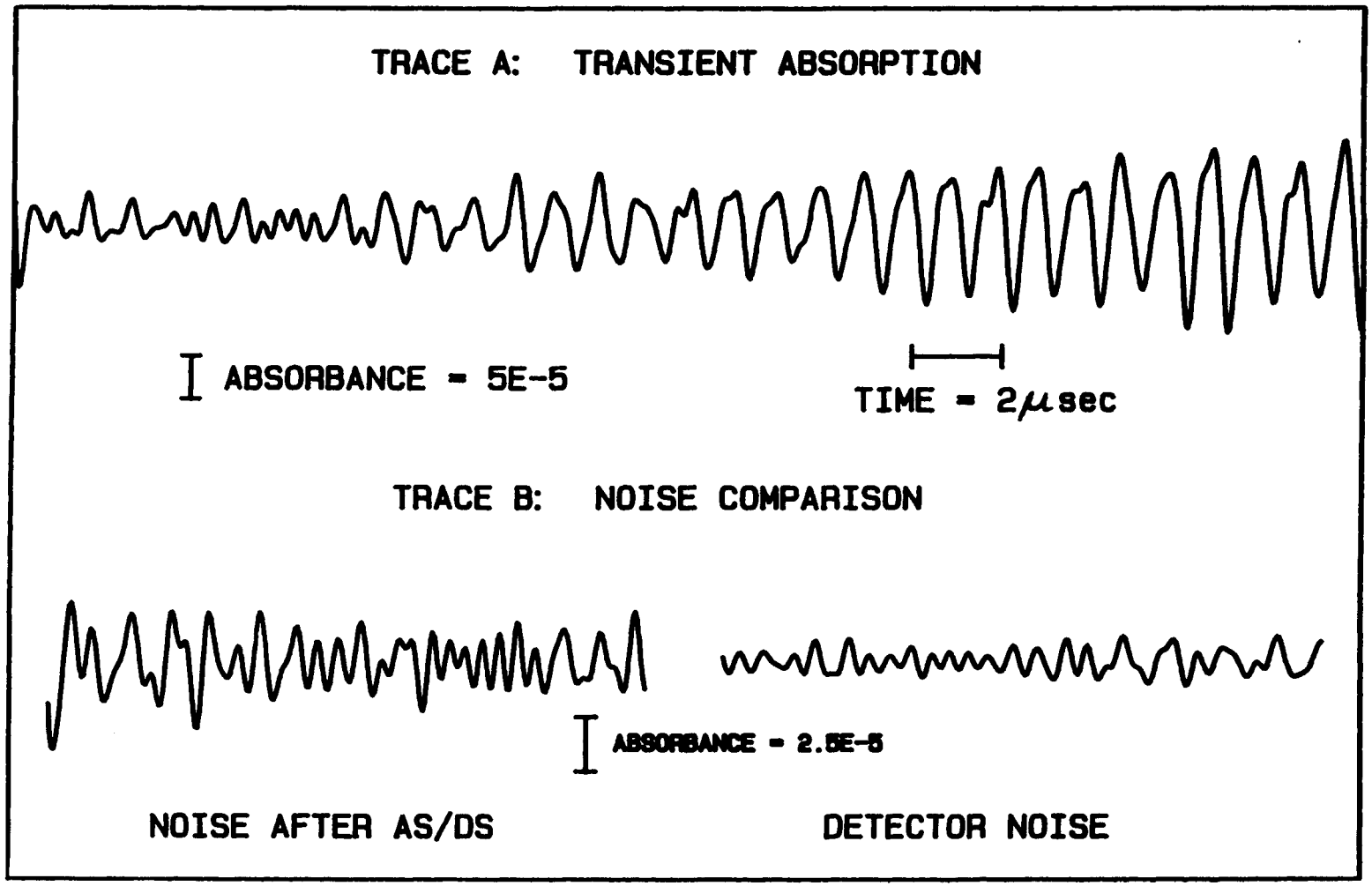
TRACE A: TRANSIENT ABSORPTION
ABSORBANCE = 5E-5
TIME = 2μsec
TRACE B: NOISE COMPARISON
ABSORBANCE = 2.5E-5
NOISE AFTER AS/DS
DETECTOR NOISE

3.5 Sensitivity of the Transient Absorption Detection Technique

The results of the previous two sections indicate that the transient detection technique is limited in sensitivity mainly by detector noise for both 100 kHz and 500 kHz TDL modulation rates. It is the purpose of this section to compare the measured value of the fractional absorption sensitivity for the 100 kHz measurements to the value calculated using the detector specifications and basic system parameters. It will be seen that the measured sensitivity is in reasonable agreement with the calculated value.

After the analog and digital subtraction steps, the root–mean–square (RMS) noise resulting from the HgCdTe detector, N_p will be given by: [23]

$$N_p = \frac{N_d G_p G_a \sqrt{BW}}{\sqrt{A_v}}$$

where N_d is the noise voltage per unit bandwidth of the detector, BW is the electronic bandwidth of the transient detection system, G_p is the voltage gain of the detector pre–amplifier, G_a is the voltage gain of the analog subtraction circuit and A_v is the number of digital averages performed. According to the detector specifications, N_d had a value of 1.44 nV/$\sqrt{\text{Hz}}$. The bandwidth of the detection system was found to be limited by the detector/pre–amplifier combination to a value of approximately 3 MHz. The voltage gain parameters were measured to be 200 for the pre–amplifier and 50 for the analog subtraction circuit. After performing 2000 digital averages (1000 averages for each record before digital

subtraction), the resultant RMS noise due to the HgCdTe detector is calculated using the expression above to be 0.56 mV. RMS calculations using the detector noise records shown in the transient absorption results section yield RMS noise voltages of 0.88 mV for the 100 kHz measurements. This measured value is in reasonable agreement with the noise voltage calculated using the previous expression.

The fractional absorption sensitivity, S, of the transient absorption detection system is given by: [23]

$$S = \frac{NEP}{P\sqrt{A_\nu}}$$

where P is the total power incident on the detector and NEP is the noise–equivalent–power of the HgCdTe detector which is defined by [19]:

$$NEP = \frac{N_d\sqrt{BW}}{R}$$

In the above expression for the noise–equivalent power, R is the value of the detector responsivity which was specified as 228 V/W. The previous two equations and the measured TDL optical power of approximately 100 μW yield a calculated fractional absorption sensitivity of 2.5×10^{-6}. Based upon the aforementioned values of the RMS detector noise voltage, the sensitivity of the transient absorption detection technique was experimentally found to be 3.5×10^{-6}. Clearly the measured sensitivity is in reasonable agreement with the calculated value. It should be noted

that the resultant noise after analog and digital subtraction revealed a sensitivity which was approximately a factor of two worse than the sensitivity measured from the corresponding detector noise record. (It is this latter sensitivity value which dictates the minimum achievable absorption signal of the detection technique.) Additional noise sources such as laser excess noise or noise resulting from optical feedback effects are probably responsible for this factor of two increase in noise.

Since the experimental results indicate that the sensitivity of the transient absorption detection technique is approximately detector noise limited, one of three possible methods should improve the achievable sensitivity. Increasing the number of records averaged, obtaining a detector with a lower noise–equivalent–power or using a TDL with a higher output power are all viable methods of improving the sensitivity of the detection technique. By employing any or all of these methods, it is hoped that the ultimate sensitivity of the transient absorption detection technique could be significantly reduced from the present equivalent absorbance detection limit of approximately 1×10^{-5}.

3.5 Summary

Techniques for monitoring transient infrared absorptions using tunable diode lasers have been described. Wavelength modulation of the TDL beam across the absorption line of interest in conjunction with both analog and digital subtraction techniques results in approximately detector–noise–limited sensitivities at both 100 kHz and 500 kHz laser modulation rates. Two methods have been described which reduce the effects of minor TDL power variations; an automated gain control circuit for the 100 kHz measurements and Fourier transform filtering

for the 500 kHz measurements. If possible, the automatic gain control loop is the preferred method for reducing the effects of the fundamental AM component since this method allows for the full use of the digital oscilloscope dynamic range.

It has been reported that FM spectroscopy in conjunction with heterodyne detection techniques has the potential to provide shot–noise limited detection combined with microsecond time resolution [9]. The transient absorption detection technique described in this chapter possesses a key advantage over these FM spectroscopy techniques. The detection technique is able to achieve a high sensitivity without sacrificing the ability to detect transients which have a fast risetime. Although sensitivities approaching 10^{-7} equivalent absorbance have been reported for two–tone FM spectroscopy [20], low–pass filter bandwidths of approximately 3 Hz were required.

At present, the transient absorption detection technique is limited in sensitivity primarily by detector noise. Thus a combination of a higher power laser, a lower noise–equivalent–power detector or an increased number of digital averages should reduce the present equivalent absorbance detection limit of approximately 1×10^{-5}. The response time of the apparatus is limited by the electronic bandwidth of the detector/pre–amplifier combination. However, lead–salt tunable diode laser have been modulated at frequencies up to several GHz [21], and hence increasing the electronic bandwidth should allow for significantly faster sampling rates. (The transient absorption detection technique requires that the TDL frequency is modulated over a significant portion of the absorption linewidth. Although the effective FM modulation index may decrease at higher modulation frequencies [22], a response time significantly shorter than 1 μsec should be achievable.) The combination of high sensitivity and fast response time provided by this technique

should prove to be extremely useful for the detection of transient infrared absorptions resulting from the creation of unstable species such as free radicals or molecular ions.

CHAPTER 4

NOISE REDUCTION TECHNIQUES FOR SPECTROSCOPY

4.1 Introduction

The implementation of high sensitivity infrared absorption spectrometers often requires the use of one or more noise reduction techniques in order to increase the signal–to–noise ratio of the detection system. Since the output powers of spectroscopic sources are finite, it is often difficult to increase the signal, and therefore the only alternative is to decrease the effects of random noise. Reduction of the effects of random noise sources can be accomplished using a variety of techniques including bandpass filtering, digital averaging, smoothing and integration. The first two techniques of noise reduction will be discussed in this chapter.

Phase–sensitive detection (PSD) techniques provided by a lock–in amplifier are commonly used for noise reduction in steady–state absorption spectroscopy. This technique relies on low–pass filtering in conjunction with heterodyne techniques to provide large signal–to–noise ratios. The bandwidth limiting method of noise reduction has been used in both transmission and harmonic spectroscopy for the implementation of high sensitivity TDL spectrometers [1,2]. Jennings' sweep integration technique [10] for high sensitivity TDL spectroscopy relies on the digital averaging approach to provide random noise reduction. A modification of this technique allowed Cassidy and Reid [11] to detect atmospheric constituents with a fractional absorption sensitivity of approximately 10^{-5}. The

digital averaging method was also instrumental in the transient absorption detection technique described in the previous chapter, where fractional absorption sensitivities approaching 10^{-5} on a microsecond time scale were reported.

This chapter, which is tutorial in nature, will involve a discussion of bandwidth reduction and digital averaging as random noise reduction techniques. Since most random noise sources can be modelled as white noise sources, a discussion on the nature of white noise is found in Section 4.2. The theory of bandwidth reduction and digital averaging noise reduction techniques, including experimental confirmation of the theory is presented in Section 4.3 and Section 4.4 respectively. Section 4.5 describes the advantages and disadvantages of these techniques for applications in absorption spectroscopy.

4.2 The Nature of White Noise

White noise is described as a random signal having a constant power spectral density (power per unit bandwidth) which is independent of frequency [23]. Such a constant spectral density over an infinite bandwidth implies an infinite power and thus the concept of white noise is not physically realizable. However, it is a useful concept if one considers the power spectral density to be constant over a certain range of frequencies and zero elsewhere – ensuring a finite total power. This is known as band–limited white noise.

Two of the most important sources of noise in electronic circuits are shot noise and thermal or Johnson noise. Shot noise results from the random arrival times of current carriers in semiconductors, whereas thermal noise is caused by thermal fluctuations of charge carriers in resistive elements [24]. The mean square

current amplitudes for each of these noise sources are given by the expressions below: [25]

SHOT NOISE $$\langle i_s^2 \rangle = 2qI_{av}\Delta f$$

THERMAL NOISE $$\langle i_{th}^2 \rangle = \frac{4kT\Delta f}{R}$$

In the above expression, q is the Coulomb constant, k is Boltzmann's constant, T is the absolute temperature, R is the resistance, I_{av} is the average current and Δf is the bandwidth. These noise sources can be considered as white noise sources since a constant power spectral density can be assigned to each quantity.

Shot noise and thermal noise sources are particularly important when choosing detectors for fibre optic communications systems. For instance, p–i–n photodiodes can achieve shot–noise–limited detection only for small bandwidth systems such as fibre optic video transmission. However high frequency, large bandwidth transmission systems using a PCM (pulse control modulation) format requires the use of avalanching devices to achieve shot–noise–limited detection [26].

For the implementation of infrared absorption spectroscopy, the optical detectors are typically liquid–nitrogen cooled photoconductive devices. (The photoconductive material HgCdTe was used for the transient absorption detection technique outlined in the previous chapter.) An analysis of the physics of the photoconductive process yields the following expression for the mean–square noise current in a frequency interval f to $f+\Delta f$: [26]

$$\langle i_p^2 \rangle = \frac{4qI_{av}(\tau_o/\tau_d)\Delta f}{1+(2\pi f\tau_o)^2}$$

/n the previous expression, τ_o is the carrier lifetime, τ_d is the carrier drift time and the other variables have been previously defined. As defined above, the generation–recombination noise associated with photoconductors violates the previous definition of band–limited white noise due to the explicit frequency dependence. However since τ_o is typically very small (~1 ns), in most cases $f\tau_o \ll 1$ and the generation–recombination noise takes the form of a modified shot noise current with a constant spectral density of $4qI_{av}(\tau_o/\tau_d)$. Thus for most applications, the photoconductive detector noise can be modelled as white noise.

The ability to model the photoconductive detector as a white noise source is an important consideration. Later in this section, a mathematical model will be developed which can be used to describe a generic white noise source. This model can be used to predict the extent to which a given technique provides noise reduction. A commercial white noise generator, which generates noise via the shot effect, can then be used to experimentally verify the theoretical predictions. Since the photoconductive detector can be modelled as a white noise source, the results outlined in this chapter are applicable to those experiments involving TDL spectroscopy which use these detectors.

A mathematical description of white noise is provided in the paper by Rice [27]. The author described white noise as a series of randomly occurring current impulses, governed by Poisson statistics and generated by the shot effect. The spectral density of the noise is derived by summing the Fourier transformed time impulses. A slightly different model which uses characteristic functions is used

in this section. The use of characteristic functions for the analysis of stochastic processes is described in a number of textbooks [23,28], and the ensuing derivation follows from Panter [23].

First consider the voltage probability distribution which results from N independent sine waves of the form:

$$x_k = A_k \sin(\theta_k)$$

where θ_k is uniformly distributed according to:

$$f(\theta_k) = \begin{cases} \frac{1}{2\pi} & \text{for } 0 \leq \theta \leq 2\pi \\ 0 & \text{otherwise} \end{cases}$$

Then, it is desired to find the probability distribution $p(z)$ where:

$$z = \sum_{k=1}^{N} x_k$$

The Fourier transform of the probability density function of the stochastic process η (where $\eta \equiv \eta(\xi)$) is called the characteristic function of η and is defined by: [28]

$$\phi(jq) = \int_{-\infty}^{+\infty} f(\xi) \exp[jq\,\eta(\xi)]\, d\xi$$

In this case:

$$\phi(jq) = \int_{0}^{2\pi} (2\pi)^{-1} \exp(iqx_k)\, d\theta_k$$

$$\phi(jq) = (2\pi)^{-1} \int_0^{2\pi} \exp\left[jqA_k \sin(\theta_k)\right] d\theta_k$$

$$= J_0(A_k q)$$

The previous equation makes use of the theory of the Bessel function [29]:

$$J_0(br) = (2\pi)^{-1} \int_0^{2\pi} \exp\left[jbr \sin(\eta)\right] d\eta$$

where $J_0(br)$ is the zeroth order Bessel function. Expanding the Bessel function in a MacLaurin series by making use of recursion relations [29]:

$$J_0(A_k q) = 1 - \frac{(A_k q)^2}{4} + \frac{(A_k q)^4}{64} + \cdots$$

Now, for $A_k q \ll 1$, one can make the approximation:

$$J_0(A_k q) \simeq 1 - \frac{(A_k q)^2}{4} \simeq \exp\left[-\frac{(A_k q)^2}{4}\right]$$

If one considers N <u>independent</u> sine waves, the characteristic function for the summation process becomes the convolution of the functions x_k [23], or in the Fourier domain:

$$\phi_\Sigma(q) = \prod_{k=1}^{N} \exp\left[-\frac{(A_k q)^2}{4}\right]$$

$$\phi_{\Sigma}(q) = \exp\left[-\frac{N(Aq)^2}{4}\right] \quad ; \text{setting } A_k = A$$

Putting this result into the standard form of a Gaussian:

$$\phi_{\Sigma}(q) = \exp\left[-\frac{\sigma_o{}^2 q^2}{2}\right] \quad ; \quad \sigma_o{}^2 = \frac{NA^2}{2}$$

In the above expression, it is clear that the square of the standard deviation is equivalent to the total mean power of N random sine waves. Therefore, without loss of generality one can set:

$$\sigma_o{}^2 = \frac{NA^2}{2} = N_o \Delta f$$

where N_o is a constant power spectral density (related to the power in one sine wave) and Δf is the system bandwidth (related to the number of sine waves contained within the frequency range). Fourier transforming back to the domain of the conjugate variable z, reveals:

$$p(z) = (2\pi\sigma_o^2)^{-1/2} \exp\left[-\frac{z^2}{2\sigma_o{}^2}\right]$$

Thus, the voltage distribution of a white noise source is a Gaussian whose squared standard deviation reveals the mean noise power contained within the bandwidth under consideration. This white noise model can now be used to explain

the bandwidth reduction and digital averaging techniques for the reduction of random noise.

4.3 Noise Reduction by Bandwidth Limiting

Direct or harmonic detection techniques in conjunction with a lock–in amplifier are often used to provide noise reduction for high sensitivity absorption spectroscopy. The function of the lock–in amplifier is essentially to limit the noise bandwidth.

The lock–in amplification process can be understood with the help of Figure 4–1. A lock–in amplifier or phase–sensitive detector simply consists of a mixer and selectable low–pass filters. A reference signal of frequency f_0 and the experimentally–derived signal are used as inputs to the mixer. The output of the mixer consists of components at the sum and difference frequencies. When the signal and the reference are at the same frequency, the output of the mixer consists of components at zero frequency and at a frequency of $2f_0$. Low–pass filtering of this mixer output signal retains only the DC component plus any noise contained within the bandwidth of the low–pass filter. The magnitude of this DC signal is dependent on the magnitude of the signal to be studied as well as the phase difference between the input and the reference signals. Proper phase adjustment of the reference signal maximizes the magnitude of the DC signal.

Mathematically, the signal power at the output of the low–pass filter, P_0 can be described by:

$$P_0 = P_{DC} + N_0 \Delta f_{LP}$$

Figure 4–1: Schematic diagram of a phase–sensitive detector. An input signal of frequency f_s is mixed with a reference signal of frequency f_o. The output of the phase–sensitive detector consists of the portion of the difference frequency which is within the bandwidth of the low–pass filter.

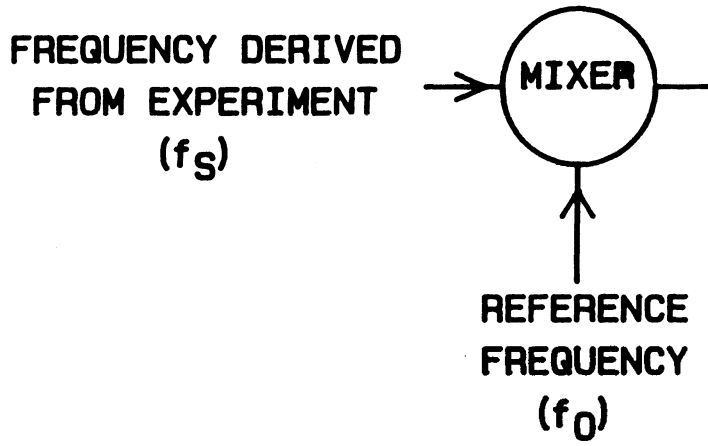
FREQUENCY DERIVED
FROM EXPERIMENT
(f_S)
MIXER
REFERENCE
FREQUENCY
(f_O)


f_S+f_O
f_S-f_O
LOW-PASS
FILTER
OUTPUT

or, since the voltage is directly proportional to the square root of the power (and the signal and noise are presumed to be uncorrelated), the signal voltage per unit resistance, S_0 can be described by:

$$S_0 = S_{DC} + \sqrt{N_0 \Delta f_{LP}}$$

where, as defined in the previous section, N_0 is the spectral density of a white noise source and Δf_{LP} is the low–pass filter bandwidth. Thus the signal–to–noise ratio is given by:

$$SNR = \frac{S_{DC}}{\sqrt{N_0 \Delta f_{LP}}}$$

Since the signal and spectral density of the noise are both presumed to be constant, the only method available for noise reduction (and a concomitant increase in *SNR*) is to reduce the bandwidth of the low–pass filter.

The bandwidth of the low–pass filter is selected using the time constant feature of the lock–in amplifier. Since the time constant and frequency bandwidth are related through the Fourier transform, an increase in the time constant corresponds to a decrease in the low–pass filter bandwidth. It is thus expected that the RMS noise voltage at the output of the lock–in amplifier varies inversely with the square root of the time constant.

In order to demonstrate the relationship between the RMS noise voltage and the lock–in time constant, the experimental apparatus shown in Figure 4–2 was used. A General Radio white noise generator was used as the input to the

Figure 4–2: Schematic diagram of the experimental apparatus used to verify the theoretical noise reduction relationships.

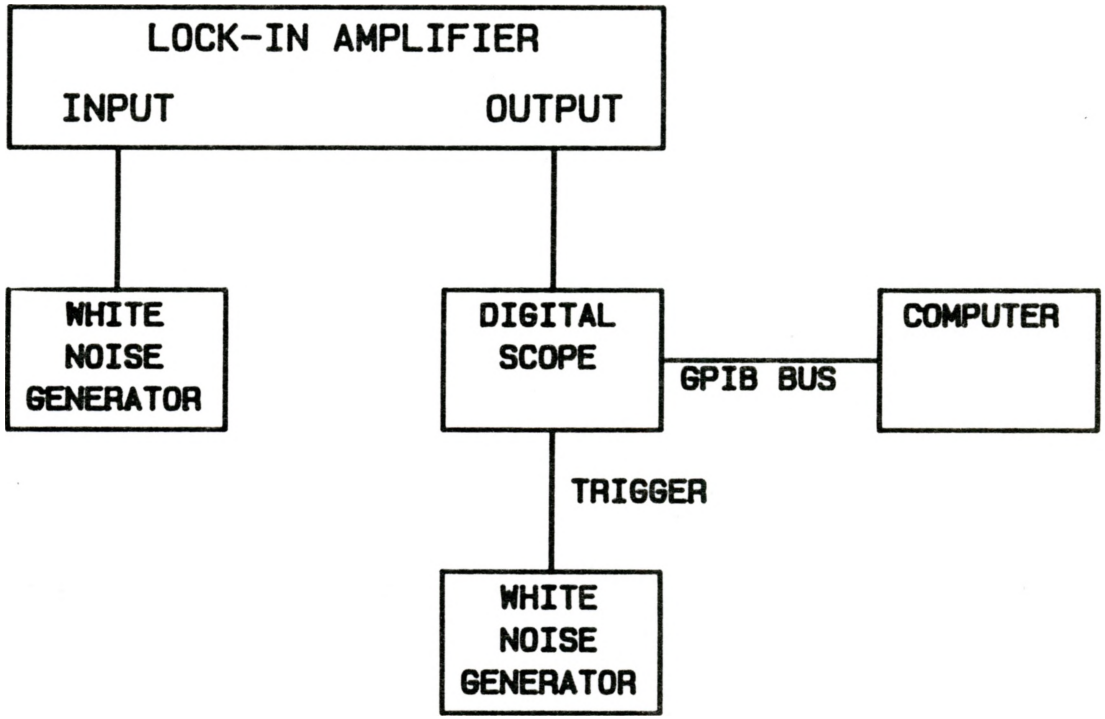
LOCK-IN AMPLIFIER
INPUT
OUTPUT
WHITE NOISE GENERATOR
DIGITAL SCOPE
COMPUTER
GPIB BUS
TRIGGER
WHITE NOISE GENERATOR

lock–in amplifier and the output voltages were monitored using a digital oscilloscope. A separate noise generator provided the oscilloscope trigger signal — ensuring that the input and trigger sources were asynchronous. One voltage value was accumulated after a time delay (between triggering events) of at least five time constants. This ensured that the voltage amplitude was able to achieve > 95% of its possible final value. Ten thousand of these points were then stored in a computer data file for further analysis. This procedure was repeated for time constants ranging from 1 ms to 1 s and for both 6 dB and 12 dB/octave filter responses.

It was previously indicated in Section 4.1 that band–limited white noise can be represented by a Gaussian voltage distribution. For a distribution having zero mean, the standard deviation of the Gaussian is identically equal to the value of the RMS voltage. Thus, the 10,000 point noise records can be analyzed by calculating the standard deviation of a best–fit Gaussian distribution. Figure 4–3 shows two examples of the Gaussian distributions obtained from an analysis of the of noise records for 3 msec and 10 msec time constants with a 6 dB/octave filter response. The Gaussian with the smaller standard deviation represents the voltage distribution after noise reduction using the 10 msec time constant. The voltage distribution for the smaller 3 msec time constant is represented by a Gaussian distribution with a larger standard deviation.

Performing the distribution analysis for the range of different time constants allowed the graph shown in Figure 4–4 to be constructed. Each data point represents the logarithm of the RMS noise voltage which is plotted as a function of the logarithm of the corresponding time constant for both 6 dB and 12 dB/octave filter responses.

Figure 4–3: Demonstration of the Gaussian voltage distribution of band–limited white noise. The voltage distribution of noise records subjected to filtering with a time constant of 3 msec is represented by the Gaussian distribution with the larger standard deviation (1.96 V). Subjecting the white noise to a filter with a larger time constant of 10 msec results in a decrease in the Gaussian standard deviation (1.25 V). The data points were obtained by generating a count versus voltage histogram for 10,000 noise voltage samples. The solid lines connecting the data points represent the best–fit Gaussian distributions which were calculated using a weighted least–squares algorithm. The inset of this figure shows 100 point portions of the 10,000 sample noise records used to generate the histogram values. (The data points and best–fit distributions have been normalized so that the areas under each Gaussian are identical.)

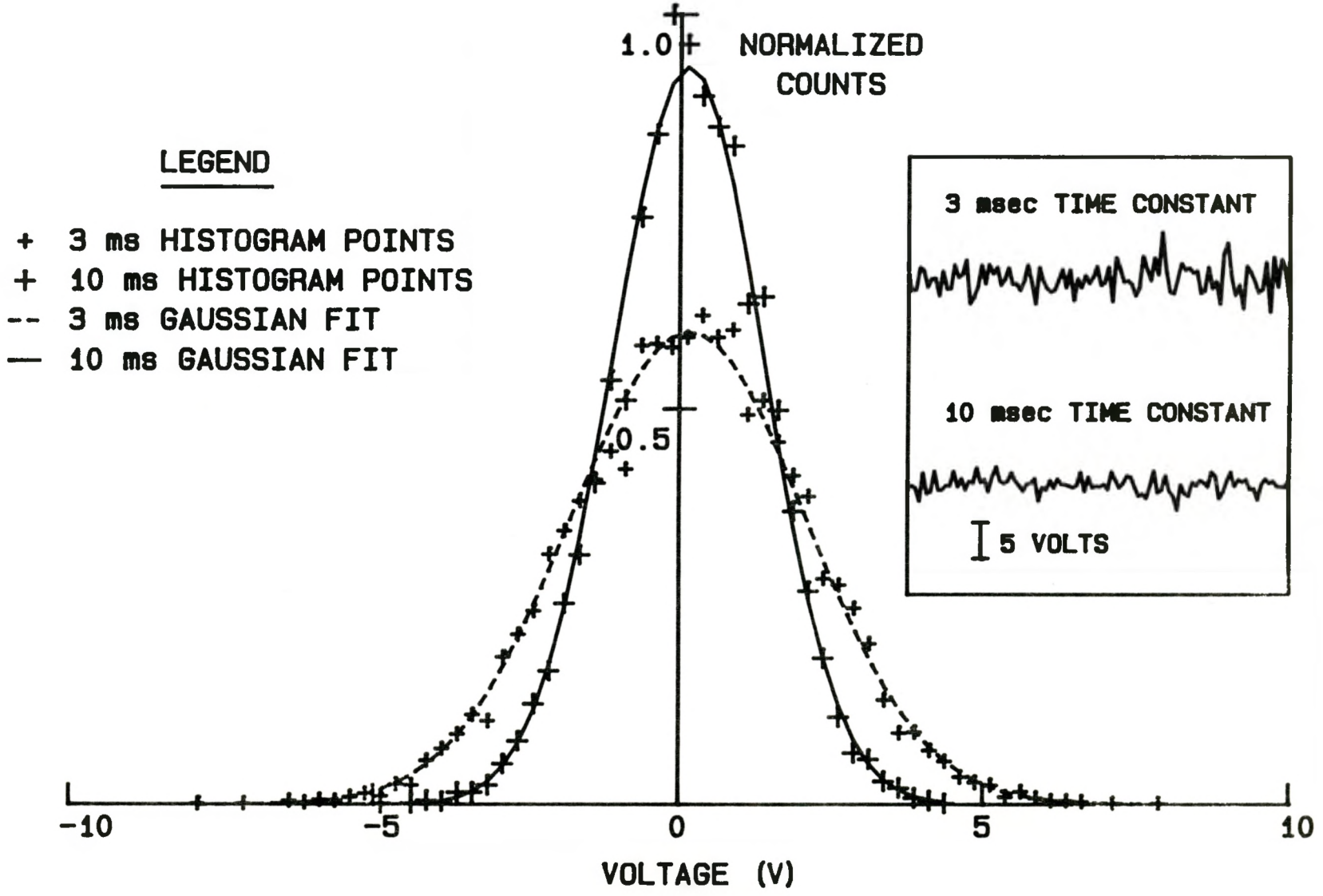
LEGEND
+ 3 ms HISTOGRAM POINTS
+ 10 ms HISTOGRAM POINTS
-- 3 ms GAUSSIAN FIT
— 10 ms GAUSSIAN FIT
1.0
NORMALIZED COUNTS
0.5
3 msec TIME CONSTANT
10 msec TIME CONSTANT
5 VOLTS
-10
-5
0
5
10
VOLTAGE (V)

Figure 4–4: Demonstration of the relationship between the RMS noise voltage at the output of the lock–in amplifier and the time constant of the low–pass filter. Plotting the logarithm of the RMS noise voltage as a function of the logarithm of the time constant yields the data points indicated on the graph for both 6 dB and 12 dB/octave filter responses. The solid lines represent linear least–squares approximations to the respective data points. Calculated values of the slopes and intercepts of the best–fit lines are also indicated on the graph.

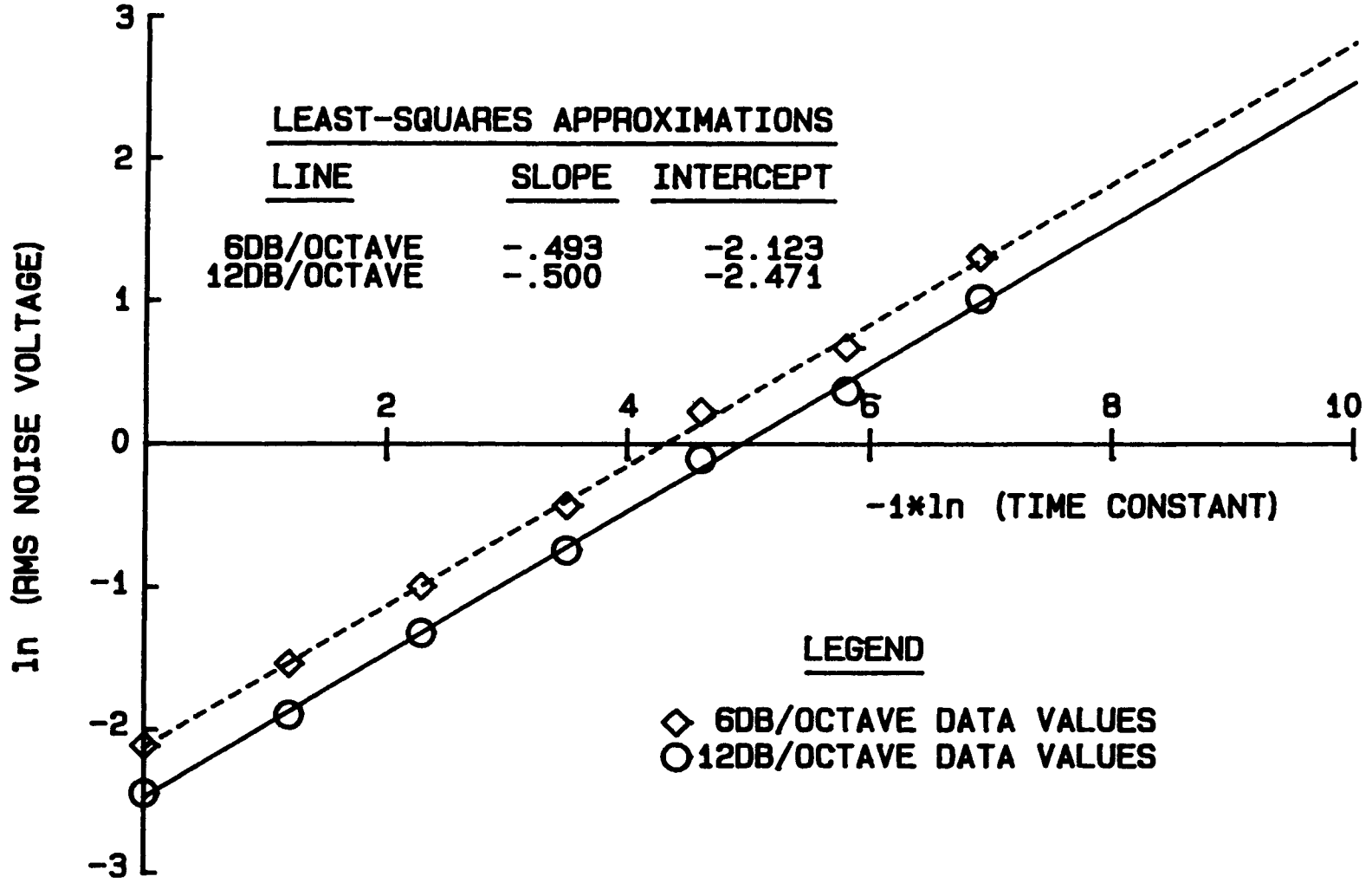
LEAST-SQUARES APPROXIMATIONS
LINE
SLOPE
INTERCEPT
6DB/OCTAVE
-.493
-2.123
12DB/OCTAVE
-.500
-2.471
ln (RMS NOISE VOLTAGE)
-1*ln (TIME CONSTANT)
3
2
1
0
-1
-2
-3
2
4
6
8
10
LEGEND
6DB/OCTAVE DATA VALUES
12DB/OCTAVE DATA VALUES

The relationship between the RMS noise voltage and the lock–in time constant was previously defined to be:

$$V_n \propto T_c^{-1/2}$$

From an analysis of the noise bandwidths for a 1–pole (6 dB/octave rolloff) and a 2–pole (12 dB/octave rolloff) filter network, it can be shown that the RMS noise voltages at the output of the low–pass filter are given by:

$$V_{n6} = kT_c^{-1/2} \qquad \text{(1–pole)}$$

$$V_{n12} = (k/\sqrt{2})T_c^{-1/2} \qquad \text{(2–pole)}$$

where k is an appropriate constant. Taking the logarithm of both sides of these equations gives:

$$\ln(V_{n6}) = \ln(k) - 1/2 \ln(T_c)$$

$$\ln(V_{n12}) = \ln(k/\sqrt{2}) - 1/2 \ln(T_c)$$

Therefore a plot of the logarithm of the RMS noise voltage versus the logarithm of the time constant should yield a linear relationship with a slope of $-1/2$. The ratio of the exponential of the intercepts for the 6 dB and 12 dB/octave filter responses should also yield a constant factor of $\sqrt{2}$.

A least–squares linear fit to the data shown in Fig. 4–4 was

calculated and the best–fit lines are shown on the graph. It can be clearly seen from the values of the slopes and intercepts of the best–fit lines (documented in Fig. 4–4) that the experimental values for the noise reduction relationships agree with the theoretical expectations.

In this section, the bandwidth reduction method of noise reduction has been examined. It has been found that the theoretical predictions for the relationship between the noise reduction and the filter bandwidth adequately describe the experimental results. Digital averaging is another method through which contributions from random noise sources can be reduced. This technique is the subject of the subsequent section.

4.4 Noise Reduction by Digital Averaging

Digital averaging is often used to provide random noise reduction in spectroscopy. It was this technique which was used to provide noise reduction in the high sensitivity transient absorption detection scheme described in the previous chapter.

The mechanism which results in the noise reduction can best be understood with a theoretical examination of the averaging process. Stated mathematically, the problem is to find the distribution of voltages $p(w)$ for the stochastic process defined by:

$$w = 1/N \sum_{i=1}^{N} z_i$$

where N is the number of averages. It was found in Section 4.2 that the noise record z_i for band–limited white noise can be described by a Gaussian distribution of the form:

$$p(z) = (2\pi\sigma_o^2)^{-1/2} \exp\left[-\frac{z^2}{2\sigma_o^2}\right]$$

Using the Fourier transform theory, the characteristic function describing each z_i is:

$$C_{z_i}(jv) = \int_{-\infty}^{+\infty} \exp\,(jvz_i)\; p(z_i)\; dz_i$$

Then, the stochastic process defined by w can be represented by the characteristic function:

$$C_w(jv) = \int_{-\infty}^{+\infty} \cdots \int_{-\infty}^{+\infty} \exp\left[jv\left(z_1/N + z_2/N + \cdots + z_N/N\right)\right] p(z_1, z_2 \cdots z_N) dz_1 dz_2 \cdots dz_N$$

Since each noise record which is to be averaged can be considered as an independent event:

$$p(z_1, z_2 \cdots z_N) = p(z_1)p(z_2)\cdots p(z_N)$$

Thus:

$$C_w(jv) = \prod_{i=1}^{N} \int_{-\infty}^{+\infty} \exp\,(jvz_i/N)\; p(z_i)\; dz_i$$

Now, since:

$$p(z_i) = (2\pi\sigma_0^2)^{-1/2} \exp\left[-\frac{z_i^2}{2\sigma_0{}^2}\right]$$

Then:

$$(2\pi\sigma_0^2)^{-1/2} \int_{-\infty}^{+\infty} \exp(\mathrm{j}vz_i/N) \exp\left[-\frac{z_i^2}{2\sigma_0{}^2}\right] \mathrm{d}z_i = 1/N \exp\left[-\frac{v^2\sigma_0{}^2}{2N^2}\right]$$

Now, taking the product of N identical terms:

$$C_w(\mathrm{j}v) = N^{-N} \exp\left[-\frac{v^2\sigma_0{}^2}{2N}\right]$$

Fourier transforming back to the domain of the conjugate variable w:

$$p(w) = (2\pi)^{-1/2}\, N^{-N} \left(\sigma_0/\sqrt{N}\right)^{-1} \exp\left[-\frac{w^2}{(2\sigma_0{}^2/N)}\right]$$

And after proper normalization such that $\int_{-\infty}^{+\infty} p(w)\mathrm{d}w = 1$:

$$p(w) = (2\pi)^{-1/2} \left(\sigma_0/\sqrt{N}\right)^{-1} \exp\left[-\frac{w^2}{(2\sigma_0{}^2/N)}\right]$$

The function of the averaging process is to return a Gaussian voltage distribution with a standard deviation of $\sigma = \sigma_0 N^{-1/2}$, where σ_0 is the standard deviation of the voltage distribution of the unaveraged white noise. Thus, the RMS voltage of the noise varies inversely with the square root of the number of averages.

The variation of the noise voltage with averaging was studied experimentally using a configuration similar to that shown in Fig. 4–2 except that the lock–in amplifier was removed from the apparatus. Thus, the signal from the white noise generator was not subjected to any low–pass filtering. After capturing a 10,000 point noise record, the digital oscilloscope then averages a predetermined number of these waveforms. A Gaussian distribution is then fit to the data using a weighted least squares algorithm. Figure 4–5 illustrates the reduction in the standard deviation of the Gaussian voltage distribution after 10 averages. As expected, the standard deviation of the averaged distribution is approximately a factor of $\sqrt{10}$ less that that of the unaveraged distribution.

Since the RMS voltage of the noise record is an estimate of the standard deviation of the voltage distribution, the noise reduction provided by the averaging process can be described by the expression:

$$V_{avg} = V_0 N^{-1/2}$$

where V_{avg} is the RMS voltage of the noise record after N averages, and V_0 is the RMS voltage of the unaveraged noise record. Thus a graph of the logarithm of V_{avg} as a function of the logarithm of N should yield a straight line with a slope of $-1/2$. Figure 4–6 shows the desired relationship. The solid line represents a least–squares approximation to the data points. The slope of this line was calculated to

Figure 4–5: Demonstration of the digital averaging noise reduction technique. The voltage distribution of the unaveraged noise record is represented by the Gaussian distribution with the larger standard deviation (82 mV). After 10 averages the standard deviation of the noise voltage distribution decreased to 26 mV. The data points indicated in the figure were obtained by generating a count versus voltage histogram for a 10,000 sample noise voltage record. The lines connecting the data points represent the best–fit Gaussian distributions which were calculated using a weighted least–squares algorithm. The inset of this figure shows 100 point portions of the 10,000 sample noise records used to generate the histogram values. (The data points and best–fit distributions have been normalized so that the areas under each Gaussian distribution are identical.)

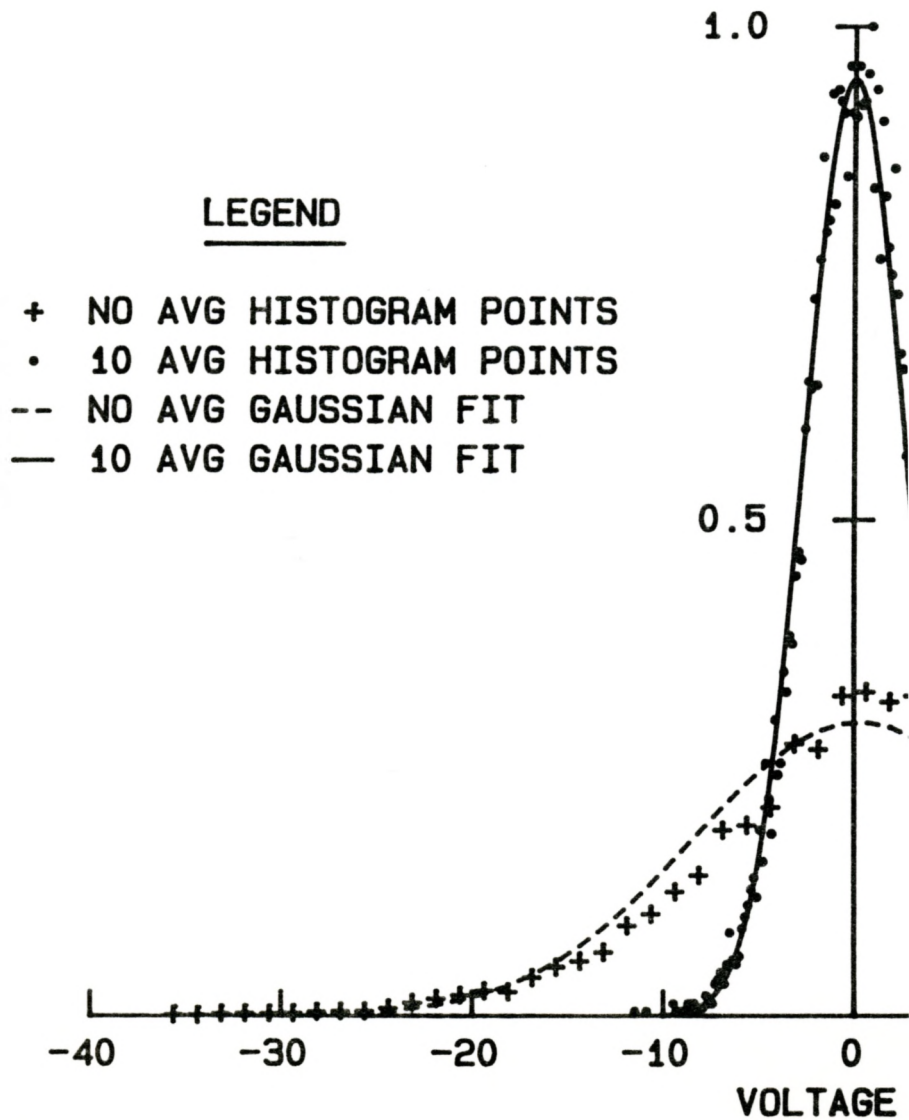
LEGEND
+ NO AVG HISTOGRAM POINTS
• 10 AVG HISTOGRAM POINTS
-- NO AVG GAUSSIAN FIT
— 10 AVG GAUSSIAN FIT
1.0
0.5
-40
-30
-20
-10
0
VOLTAGE

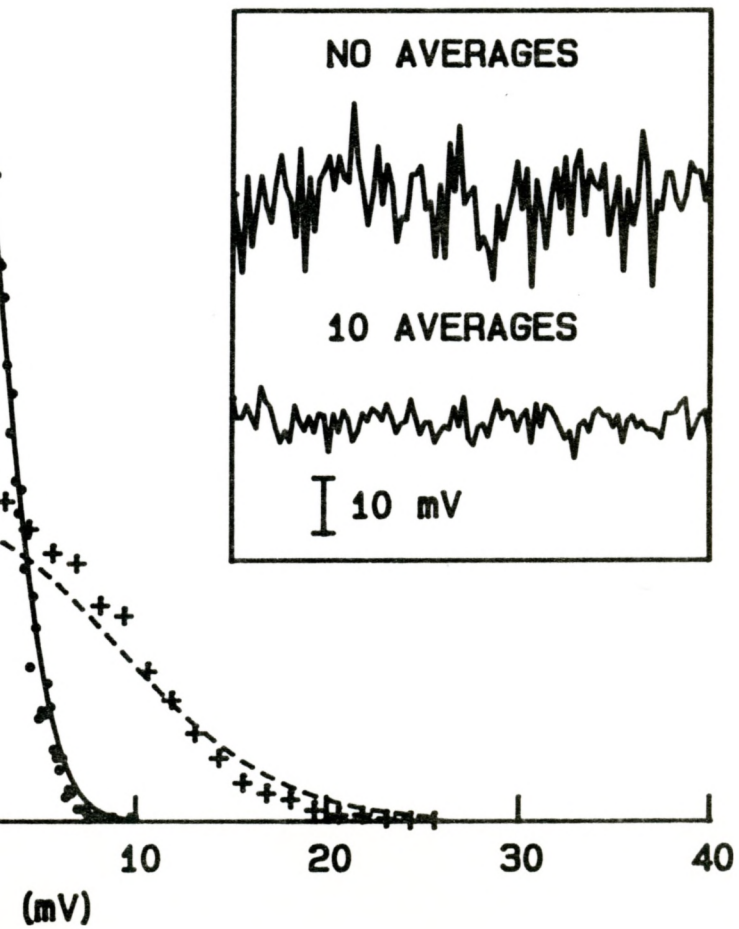
NORMALIZED
COUNTS
NO AVERAGES
10 AVERAGES
10 mV
10
20
30
40
(mV)

Figure 4–6: Demonstration of the relationship between the RMS noise voltage and the number of digital averages. Plotting the logarithm of the RMS noise voltage as a function of the logarithm of the number of digital averages yields the data points indicated on the graph. The solid line represents a linear least–squares approximation to the data points.

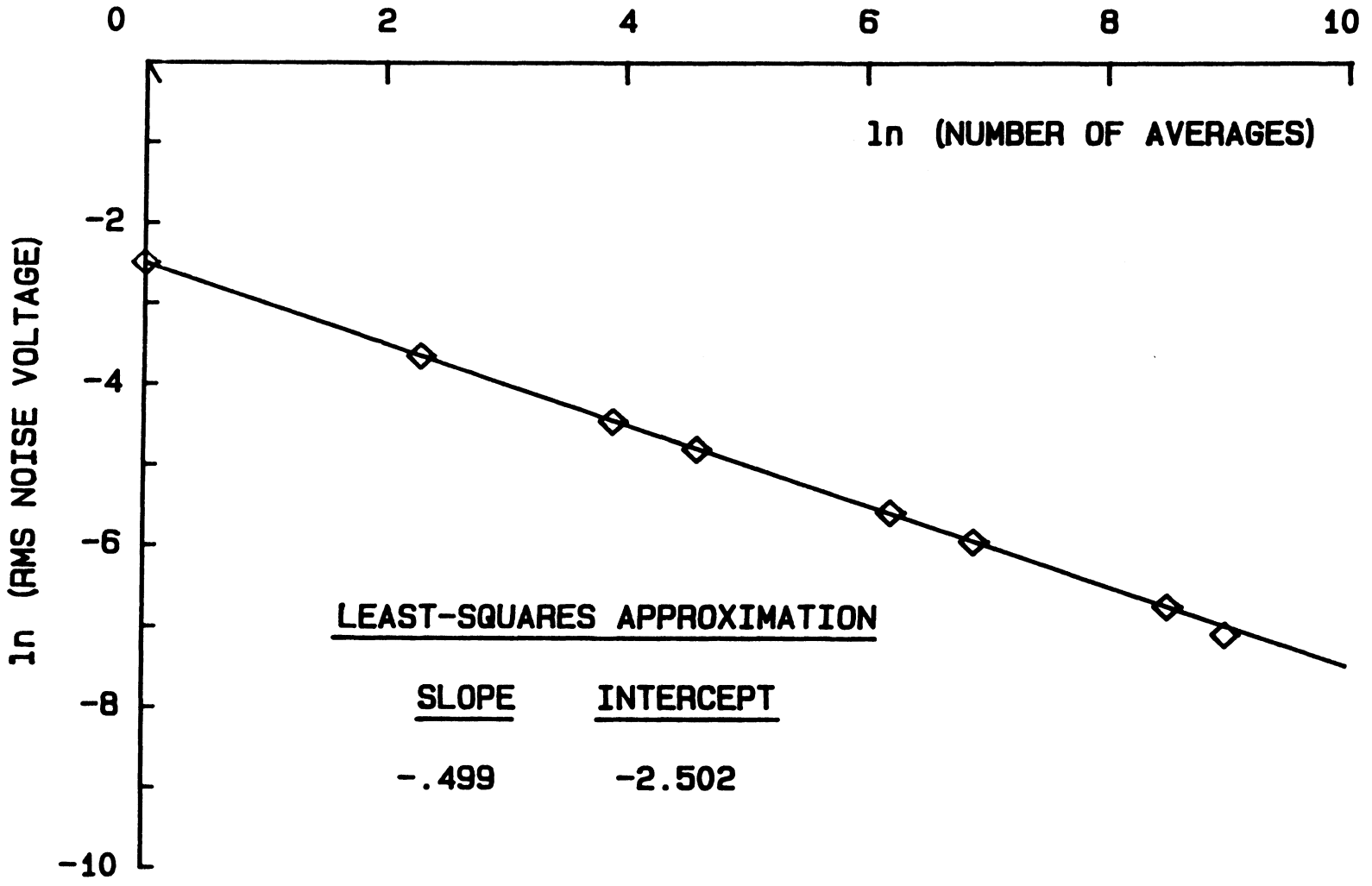
0
2
4
6
8
10
ln (NUMBER OF AVERAGES)
-2
-4
-6
-8
-10
ln (RMS NOISE VOLTAGE)
LEAST-SQUARES APPROXIMATION
SLOPE
INTERCEPT
-.499
-2.502

be –0.499, which is in excellent agreement with the theoretical prediction.

In this section, the digital averaging approach to the reduction of random noise has been examined both theoretically and experimentally. Using an analysis based on the use of characteristic functions, the RMS noise voltage was found to be inversely proportional to the square root of the number of averages. The averaging of noise records from a white noise generator revealed results which were in excellent agreement with the theoretical predictions.

4.5 Bandwidth Reduction versus Digital Averaging

In the previous two sections, the theoretical aspects of bandwidth reduction and averaging as methods of random noise reduction were examined. It was found that the RMS noise voltage varies linearly with the square root of the bandwidth and inversely with the square root of the number of signal averages. Each of these relationships was experimentally confirmed using a white noise generator, a lock–in amplifier and a digital oscilloscope. It is the purpose of this section to compare the bandwidth reduction and averaging techniques so that one can assess the advantages or disadvantages of a given technique when designing an optimized TDL spectrometer.

The bandwidth reduction method of reducing the effects of random noise has historically been exploited in the areas of transmission and harmonic spectroscopy using Pb–salt tunable diode lasers. For instance, using second harmonic techniques, Reid et al [1] were able to detect steady–state absorptions with an absorption sensitivity of approximately 10^{-5}. Noise reduction was provided by a lock–in amplifier with a low–pass filter time constant of 1 second. Using

higher power lasers, Cooper and Carlisle [20] demonstrated and absorption sensitivity of $\sim 2 \times 10^{-7}$ using single and two–tone frequency modulation techniques. These authors implemented a low–pass filter bandwidth of 2.44 Hz (time constant of ~65 ms) to achieve the reported sensitivity.

The high sensitivities reported in the previous paragraph indicate the need for small bandwidth (long time constant) low–pass filters when a phase–sensitive detection technique is adopted. These small bandwidth detection systems are adequate for steady–state absorption detection. Unfortunately, the bandwidth limiting approach to noise reduction is wholly inadequate for a transient absorption detection system where the absorptions change on a millisecond time scale. For instance, an absorption which changes on a time scale of about 160 ms cannot be detected in a 1 Hz bandwidth.

The sweep integration technique pioneered by Jennings [10] and modified by Cassidy and Reid [11] uses the averaging method to provide noise reduction. The latter authors were able to achieve steady–state absorption sensitivities approaching 10^{-5} using this averaging technique. Using a high speed version of the sweep integration technique, the results outlined in Chapter 3 indicate a TDL spectrometer capable of achieving absorption sensitivities of 10^{-5} while simultaneously tracking absorptions which change on a microsecond time scale. Thus, the digital averaging approach to noise reduction allows for high sensitivity detection without sacrificing fast response times. In fact, the ultimate response time of the digital averaging technique is dependent on the sampling rate of the oscilloscope analog–to–digital converter.

From the results of the previous section, it seems that by simply increasing the number of waveforms which are averaged, random noise can be

reduced to any required level. Practical considerations however, impose a limit to the number of waveforms which can be averaged in a realistic detection system. Often the limiting noise in an experiment is composed of a number of independent noise sources. For example, in the case of the transient absorption detection technique, averaging can only reduce those noise sources which are incoherent with respect to the laser modulation signal. As the effect of these incoherent noise sources are reduced, the presence of coherent signals, such as those caused by laser feedback effects (fringes), may impose a limit to the sensitivity of the spectrometer.

The ability of the averaging technique to improve detection sensitivity relies on the fact that signals such as absorption lines can be accurately overlayed in memory whereas incoherent signals cannot. For the transient absorption detection experiment, accurate overlaying of absorption lines requires both a stable trigger and a laser frequency which does not drift within the time required to average the waveforms. Clearly, a trigger signal which jitters or a drift in the laser wavelength would result in a broadening of the detected absorption line and a concomitant decrease in signal–to–noise ratio.

Assuming a stable trigger can be provided, it is likely that the TDL wavelength drift would impose a practical limit to the number of waveforms which could be averaged. The digital oscilloscope used in the transient absorption detection experiment has the ability to average waveforms at a rate of ~30 Hz. Thus 1,000 averages requires about 30 seconds of processing time. If a 10–fold increase in sensitivity were desired, 1×10^5 averages would be required, necessitating approximately 1 hour of processing time. It would be very difficult to maintain the wavelength stability of the TDL over this time period. It should be noted that this wavelength drift can also impose a practical limit to the low–pass filter bandwidth

which can be used for noise reduction in PSD–based TDL spectrometers. In order to provide very small noise voltages, small bandwidth filters are required, and the TDL must sweep slowly across the absorption feature of interest. If the laser wavelenth drifts during this sweep interval, it is clear that a degradation in signal quality will occur.

It seems that the sweep integration or averaging technique used to provide noise reduction in TDL spectrometers is more versatile than the bandwidth reduction technique. Digital averaging has the ability to provide noise reduction without sacrificing a fast response time. The bandwidth reduction technique cannot provide both of these attributes and is therefore only suitable for the detection of steady–state absorption lines.

4.6 Summary

Two different techniques which are commonly used for the reduction of random noise in laser spectrometers have been examined in this chapter. Experimentally obtained relationships verified the theoretical dependencies which were derived for both the bandwidth limiting method of noise reduction (often used in phase sensitive detection techniques) and the digital averaging technique. It was the latter technique which provided the required noise reduction for the transient absorption detection method described in the body of this thesis. Comparing the methods of random noise reduction, it was concluded that the digital averaging technique is the most versatile since it provides for high sensitivity detection without sacrificing the fast response time required for transient absorption measurements.

CHAPTER 5

CONCLUSION

The major portion of the work reported in this thesis has concerned the development and implementation of a high speed, high sensitivity technique for the monitoring of transient infrared absorptions using lead–salt tunable diode lasers. It was reported that this technique has the ability to monitor transient absorptions which change on a microsecond time scale as well as providing fractional absorption sensitivities of $\sim 1\times10^{-5}$. These two attributes result in a transient absorption detection technique which is thought to be superior to both FM heterodyne [9] and gated–integration [6] techniques.

The transient absorption detection technique is limited in sensitivity mainly by detector noise. Thus, a combination of either a higher power lead–salt diode laser or a detector with a lower noise–equivalent–power should improve the sensitivity to a value below the present limit of $\sim 10^{-5}$ equivalent absorbance. In terms of response time, the present technique is limited by the bandwidth of the detector/pre–amplifier combination. Detector electronics with a larger bandwidth should allow for absorption sampling times into the nanosecond regime.

The transient absorption detection technique developed during the course of this study should prove to be extremely useful to spectroscopists wishing to study the absorption spectra of unstable species. Logical extensions to the work reported in this thesis include studies of transient species such as free radicals and molecular ions. In particular, it is hoped that the transient absorption detection technique could provide new insight into the kinetics of reactions in the areas of

atmospheric and interstellar chemistry, biology, and semiconductor materials processing.

REFERENCES

1. J. Reid, M. El–Sherbiny, B.K. Garside and E.A. Ballik, "Sensitivity limits of a tunable diode laser spectrometer, with application to the detection of NO_2 at the 100–ppt level", Appl.Opt. 19, 3349–3354 (1980).

2. D.T. Cassidy and J. Reid, "Atmospheric pressure monitoring of trace gases using tunable diode lasers", Appl.Opt. 21, 1185–1190 (1982).

3. C.R. Webster and R.T. Menzies, "In situ measurements of stratospheric nitric oxide using a balloon–borne diode laser spectrometer", Appl.Opt. 23, 1140–1142 (1984).

4. G.A. Laguna and S.L. Baughcum, "Real–time detection of methyl radicals by diode laser absorption at 608 cm^{-1}", Chem.Phys.Lett. 88, 568–571 (1982).

5. D. Harradine, B. Foy, L. Laux, M. Dubs and J.I. Steinfeld, "Infrared double resonance of fluoroform–d with a tunable diode laser", J.Chem.Phys. 4267–4279 (1984).

6. H. Kanamori, J.E. Butler, K. Kawaguchi, C. Yamada and E. Hirota, "Infrared diode laser kinetic spectroscopy of transient molecules produced by excimer laser photolysis", J.Mol.Spectrosc. 113, 262–268 (1985).

7. E. Hirota, High–resolution spectroscopy of transient molecules, Springer–Verlag, Berlin, Germany, 1985.

8. D.J. Danagher and J. Reid, "Vibrational relaxation of the ν_2=1 level of ortho and para NH_3", J.Chem.Phys. 86, 5449–5455 (1987).

9. M. Gehrtz, W. Lenth, A.T. Young and H.S. Johnston, "High–frequency–modulation spectroscopy with a lead–salt diode laser", Opt.Lett. 11, 132–134 (1986).

10. D.E. Jennings, "Absolute line strengths in ν_4, $^{12}CH_4$: A dual–beam diode laser spectrometer with sweep integration", Appl.Opt. 19, 2695–2700 (1980).

11. D.T. Cassidy and J. Reid, "High sensitivity detection of trace gases using sweep integration and tunable diode lasers", Appl.Opt. 21, 2527–2530 (1982).

12. D.T. Cassidy, "Trace gas detection using 1.3 μm InGaAsP diode laser transmitter modules", Appl.Opt. 27, 610–614 (1988).

13. H. Preier, "Recent advances in lead–chalcogenide diode lasers", Appl.Phys. 20, 189–206 (1970).

14. R.S. Eng, J.F. Butler and K.J. Linden, "Tunable diode laser spectroscopy: an invited review", Opt.Eng. 19, 945–960 (1980).

15. G.P. Agrawal and N.K. Dutta, Long–wavelength semiconductor lasers, Van Nostrand Reinhold Co., New York, 1986.

16. P.H. Beckwith, C.E. Brown, D.J. Danagher, D.R. Smith and J. Reid, "High sensitivity detection of transient infrared absorptions using tunable diode lasers", Appl.Opt. 26, 2643–2649 (1987).

17. G. Guelachvili and K.N. Rao, Handbook of infrared standards, Academic Press Inc., Orlando, 1986.

18. K.E. Fox and J. Reid, "Dynamics of the N_2O laser as measured with a tunable diode laser", J.Opt.Soc.Am. B2, 807–814 (1985).

19. K. Shimoda, "Limits of sensitivity of laser spectrometers", Appl.Phys. 1, 77–86 (1973).

20. D.E. Cooper and C.B. Carlisle, "High sensitivity frequency modulation with a lead–salt diode laser", private communication.

21. D.E. Cooper and R.E. Warren, "Two–tone optical heterodyne spectroscopy with diode lasers: theory of line shapes and experimental results", J.Opt.Soc.Am B4, 470–480 (1987).

22. S. Kobayashi, Y. Yamamoto, M. Ito and T. Kimura, "Direct frequency modulation in AlGaAs semiconductor lasers", IEEE J.Quant.Electron. QE–18, 582–595 (1982).

23. P.F. Panter, Modulation, noise and spectral analysis, McGraw–Hill Book Co., New York, 1965.

24. J. Millman and C.C. Halkias, Integrated electronics, McGraw–Hill Book Co., New York, 1972.

25. S.M. Sze, Physics of semiconductor devices, John Wiley and Sons, New York, 1981.

26. A. Yariv, Introduction to Optical Electronics, Holt, Rinehart and Wilson, New York, 1976.

27. S.O. Rice, "Mathematical analysis of random noise", Bell Syst.Tech.J. 23, 282–332 1945.

28. A. Papoulis, Probability, random variables and stochastic processes, McGraw–Hill Book Co., New York, 1965.

29. G. Arfken, Mathematical methods for physicists, Academic Press Inc., New York, 1970.